JOURNAL OF MATERIALS SCIENCE 32 (1997) 1673–1692

Review
Ceramic tensile strength–grain size relations: grain sizes, slopes, and branch intersections

R. W. RICE
5411 Hopark Drive, Alexandria, VA 2310, USA

The use of the average or maximum grain size, G, in G–tensile strength, σ, relations and the resultant character of the σ-$G^{-1/2}$ plots have been considered. Experimental and literature data (mainly at 22 °C) show that using the size of exaggerated grains in Al_2O_3, β-Al_2O_3, B_4C, SiC, Si_3N_4 and probably TiO_2 (i.e. mainly non-cubic materials), is appropriate, provided such grains are the source of failure and are larger than or equal to the flaw size, which is most probable at intermediate G, otherwise an average G, G_a, is appropriate. Larger grains or clusters of larger grains do not always act as fracture origins, because associated flaws, mainly cracks (e.g. from machining) or pores are required. G_a was found to be appropriate for materials (e.g. MgO, Y_2O_3, ZrO_2 and $MgAl_2O_4$) not typically having exaggerated grains. The slopes of the larger and finer G branches of the σ–$G^{-1/2}$ plots are shown to be less than for polycrystalline K_{IC} and more than 0, respectively, contrary to assertions of other workers using maximum G, G_m. The latter slope indicates that the R-curve effects and related mechanisms have much more limited effects on σ than is commonly recognized. Better measurement and characterization needs are identified, i.e. (1) basic consistency between σ and G values (violated in the past use of G_m), and (2) addressing the spatial distribution of larger grains and other defects, e.g. via fractography. Use of an average (possibly weighted) grain diameter for G instead of a linear intercept, is recommended.

1. Introduction

The grain size; G, dependence of flexure (tensile) strength, σ, is important as both a guide in developing materials of higher or more reliable σ, and understanding mechanisms of failure, usually via analysis of σ–$G^{-1/2}$ behaviour. While standard procedures for determining σ and G at first appear to be adequate, the situation can be more complex. A key factor in this complexity is which G to use. While an average G, G_a has been almost universally used [1–7], a few investigators have used a maximum G, G_m [8–13], prompted by (1) σ generally decreasing with increasing G and tensile failure being a weak link process, and (2) observations of fracture origins being from larger grains (mainly in Al_2O_3 [3–7]). However, all studies using G_m have been limited; only two [8, 11] using G_m presented even limited fractographic corroboration of failure from large grains, and none made significant comparison to other data.

The impact and complexity of which G to use can be seen by considering the two basic σ–$G^{-1/2}$ regimes for ceramics failing from flaws [1–13] (Fig. 1). For the finer G branch(es), where the flaw size, C is more than G, varying values of C lead to either scatter and a resultant broad branch, or different branches in either case with limited G-dependence of σ. The larger G branch, where (the initial) $C \leqslant G$, (1) has a substantial positive slope (more than that of the finer G branch(es)), and (2) commonly extends to polycrystalline strengths well below those for the weakest single crystal orientation(s) with comparable surface finish. (In the limited cases where slip nucleates fracture, e.g. CaO and MgO [4, 5, 7], there may be only one σ–$G^{-1/2}$ branch, intersecting the σ axis at approximately the yield stress, or this exists at larger G, shifting at finer G to flaw failure branches like those discussed above.) The G value used can determine the branch on which a σ value is plotted and has a significant impact on larger and finer σ–$G^{-1/2}$ branch slopes (generally increased by use of G_m), which are basic to interpreting mechanisms and projecting σ improvements from reduced G. However, the flaw argument for use of G_m is pertinent only so long as flaws are associated with G_m and $G_m \geqslant C$ (initial and final). G can also affect σ via K_{IC}, but where it does, K_{IC} is affected more by G_a than G_m and generally decreases with decreasing G [4, 14], hence possibly emphasizing smaller, not larger, G values.

However, some investigators using G_m have assumed that the σ–$G^{-1/2}$ slope of the (1) larger G branch is the polycrystalline K_{IC} (and goes through the axis origin [8–10, 12]), and (2) finer G branch(es) = zero [8–10].

This paper presents both data and analysis on the use of G_m, focusing particularly on those materials where G_m has been used. It is shown that use of G_m

0022–2461

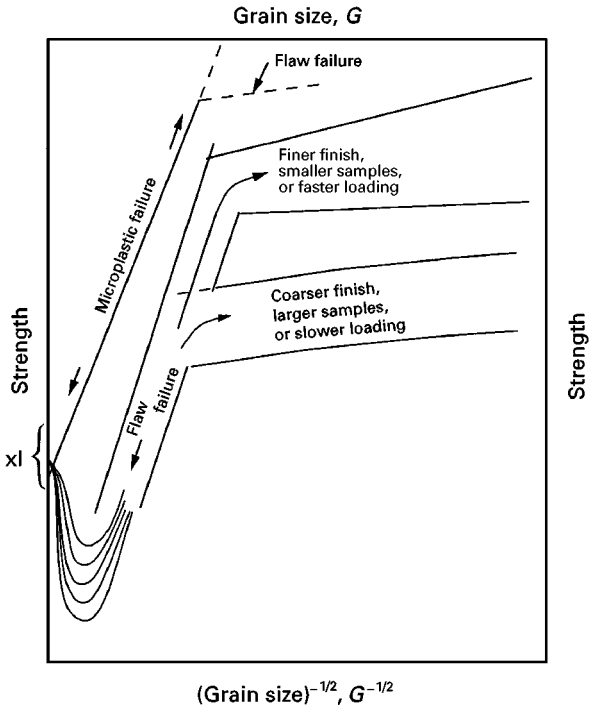

Figure 1 Schematic illustration of ceramics strength–grain-size behaviour. The uppermost, microplastic, curve extrapolates at infinite G to the activation stress for the easiest activated microplasticity. At finer G, i.e. higher σ, branching to a reduced G dependence of σ, can occur due to flaws whose size, C, is $> G$. Lower curves show the two-branch behaviour of typical brittle, flaw-controlled failure. The two finer G branches reflect different flaw populations, both with $C > G$. Greater G dependence of σ commences when $C \leqslant G$. As G increases, a further transition must occur to the σ of comparably finished single-crystal specimens. Although single crystal σs (xl) are orientation dependent, the weakest orientations generally have $> \sigma$ values than larger G polycrystals. (The use of one crystal σ range for both microplastic and brittle failure is for schematic simplicity and is not meant to imply that these values are similar for the same or different material systems.)

is an oversimplification, being appropriate in only certain ranges of particular materials, and even then not universally so. Slopes of larger G branches are shown to generally be $< K_{IC}$ (polycrystalline). Finer G branch slopes are shown to generally be > 0, even when using G_m (as they typically are using G_a [1–7]), a trend not directly consistent with many K_{IC}–G data and large-scale cracking, e.g. R-curve and bridging, phenomena [14, 15]. Related G distribution and measurement issues are also addressed, i.e. where the G distribution is of importance, so may be the spatial distribution of larger grains as well as other associated defects, especially pores.

2. Experimental and analytical procedure

Either of two commercial Al_2O_3 powders designated A and B (Linde A and Linde B powders from the Linde Company, Speedway, Indiana), were hot pressed in graphite dies, typically at 1400–1600 °C for 30–90 min with 35 MPa pressure as described in detail elsewhere [16]. Rectangular bars ($\sim$ 2.5 mm thick and $\sim$5 mm wide) were diamond sawn and ground (parallel with the bar axis, unless noted otherwise) from the $\sim$ 3.8 cm diameter, $\sim$ 6 mm thick discs, most commonly cut with their widths parallel to the disc pressing direction. Specimens were also machined from commercial 96% and 99% Al_2O_3bodies (respctively, Alsimag-614 and an experimental body from American Lava incorporated), and various hot-pressed B_4C as previously discussed [17]. All bars were tested with rounded edges at nominally 22 °C and 40% RH (using three-point flexure, typically with a span-to-thickness ratio of 6) and a head travel rate of 1.25 mm min^{-1}.

Fractures were examined [18, 19] to determine fracture origin location and character. Strengths were corrected for failure being either off-centre or into the depth of the sample, based upon expected linear stress gradients. G was taken as the average of the grain diameters exposed on the fracture surface at, or in the vicinity of, the fracture origin. Where grains were significantly non-equiaxed, the G value is the diameter of the circle having the same area as that of the grain exposed on the fracture surface. Whether a G value was the flaw size or a major portion of it was based on it yielding approximately the polycrystalline K_{IC} value in

$$K_{IC} = \frac{\sigma C^{1/2}}{Y} \quad (1)$$

using $G/2 = C$ the factor 1/2 occurs because G is a diameter and C a radius, where C is the radius of a semi- or full-circle having the same area as the respective surface or interior flaw, and Y is the geometrical factor: 0.79, 0.74 and 0.62, respectively, for surface (half-penny), corner (quarter-penny), and internal (full-penny) flaws. Similarly, C at the larger G–finer G branch intersections was calculated from Equation 1 using the σ at the intersection.

3. Results and discussion

3.1. Al_2O_3

Fig. 2 shows machined, hot-pressed $Al_2O_3\sigma$ versus G_a, as well as G_m, where there was one or more large grains that could have been the fracture origin; typically exaggerated grains, i.e. not part of the main grain distribution as shown by their size, and common shape (e.g. tabular platelets). Results were also distinguished by whether the fracture initiated from the tensile surface of the specimen or its edge (i.e. from the corner of the fracture surface). The primary result of this use of G_m was to transfer 16 of 40 data points from the finer to the larger G branch, increasing both the slope of the large G branch and the σ level to which it extends. However, the resultant large G branch slope is still less than the polycrystalline K_{IC} (Table I). Otherwise, use of G_m (for exaggerated grains) does not significantly change the range or scatter of the data, or the trend for lower σ failures from the edge of the samples versus the tensile surface (which is consistent with MgO data [20]). It provides no clear support for zero slope(s) for finer G branch(es) (e.g. for edge and tensile surface failures) in fact indicating positive slope(s), and neither proves nor disproves a zero intercept from extrapolating the large G branch to $\sigma = 0$.

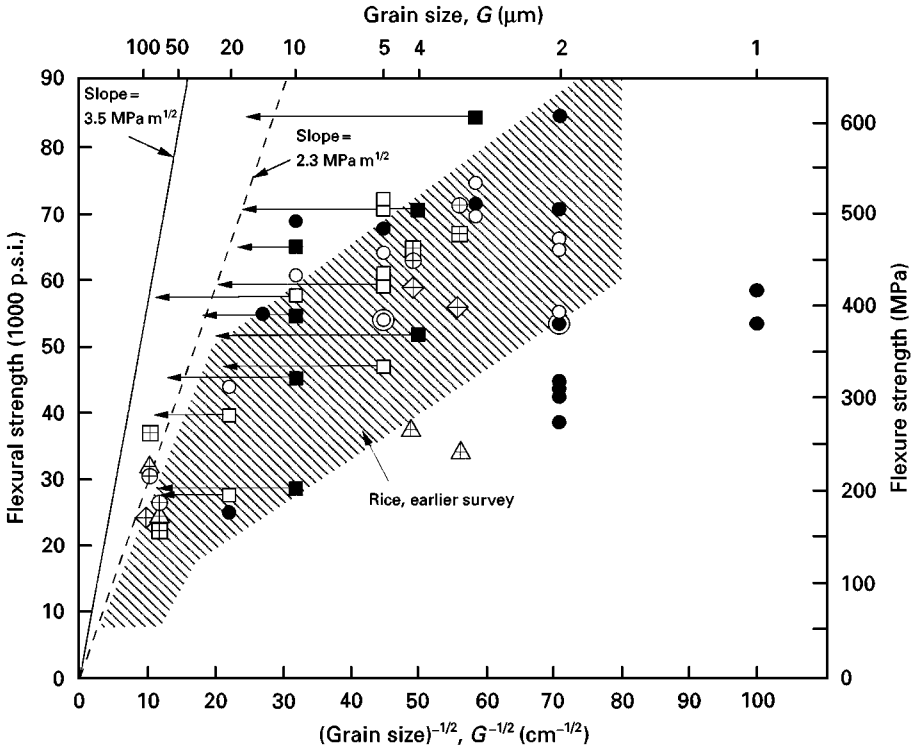

Figure 2 σ–$G^{-1/2}$ data for machined, hot-pressed Al_2O_3 at 22 °C. Note designation of failure initiated from (○, □) the tensile surface or (●, ■) the corner of the fracture (i.e. the specimen edge) and whether the origin occurred from a region of (○, ●) essentially normal grain structure or (□, ■) with one or more exaggerated grains. All data are plotted versus G_a, where failure involved exaggerated grains, the arrow tip indicates that size, i.e. G_m. Hot-pressed Al_2O_3 data of Tressler *et al.* [8] are plotted versus their G_m values for the various grifts used in machining (perpendicular to the specimen tensile axis): (△) 220 gnt, (◆) 400 gnt, (■) 600 gnt, (⊕ 1/4 μm. The crosshatched region shows the range of Al_2O_3 data from a previous survey [3]. Slope of 3.5 and 2.3 MPam$^{-1/2}$ are in terms of G, and must be reduced to 71% of these values to reflect K_{IC} (i.e. due to C being a radius where as G is a diameter).

TABLE I Slope and intersection analysis of σ–G data

Material (Fig.)	K_{IC} MPam$^{1/3}$	Larger G slope (MPam$^{1/2}$)[a]	Larger–finer G branch intersection		
			σ(MPa)	G(μm)	C(μm)[b]
Al_2O_3 (2)	3.5	2.3 (1.6)	~ 350	35	62 (25)
Al_2O_3 (3)	3.5	2.6 (1.8)	~ 400	50	48 (19)
Survey Al_2O_3 (2, 3)	3.5	2.0 (1.4)	400	30	48 (19)
Al_2O_3 (Alford et al.) (5)	3.5	3.2 (2.3)	940	25	
Al_2O_3 W (6)	~ 3.5	2.3 (1.6)	350	70	62 (25)
β Al_2O_3 (13)	~ 3.2	1.9 (1.3)	180	120	197 (79)
TiO_2 (14)	1.6	1.6 (1.1)	270	35	21 (9)
		(1.2 (0.8)	(400)	(10)	10 (4)
TiO_2 (Alford *et al.*) (14)	1.6	1.6 (1.1)	770	45	
B_4C (7)	3.3	2.0 (1.4)	370	40	50 (20)
SiC (15)	3.5	3.3 (2.3)	360	70	59 (24)
			850	7	9 (4)
SiC (16)	~ 3.5	⩽ 3.5 (2.5)	–	–	–
Si_3N_4 (17)	⩾ 4	⩽ 4 (2.9)	–	–	–

[a] The second value shown horizontally in parentheses is the slope multiplied by 0.71 to convert to a K_{IC} value because G is a diameter and C a radius (i.e. $C \sim G/2$). Values under the first set are for alternative interpretations where they existed.

[b] Values shown are for a surface half-penny crack. Values in parentheses are for a slit crack to give a feeling for some elongation of the flaw, within the constraints of the grain size and shape (and also would commonly be somewhat greater than half-penny crack radii based on single-crystal K_{IC} values).

Tressler *et al.* [8] used Al_2O_3 hot pressed with MgO ($G_a \sim 2$ μm) or without MgO (G_as ~ 3, 12, or 18 μm) ground parallel with the bar axis, air annealed (4 h, 1000 °C), then re-machined perpendicular to the bar axis with various grits (Fig. 2). Their data generally agree well with the other data of Fig. 2 whether plotted versus G_a or, as they did, versus G_m($G_m \sim 3.3$ and 4.3 μm for the two finest G bodies, but ~ 80–100 μm, owing to scattered large platy grains found at fracture origins in their two largest G bodies).

Subsequent data of the present study for machined samples of (1) hot-pressed (without additives), (2) sintered Al_2O_3 failing from large isolated or clustered large grains, and (3) two previous large G failures [21] in hot-pressed Al_2O_3(+ 0.5% MgO) [21], plotted versus G_a and G_m and (for clusters) the cluster size at the fracture origin, agree with the above data and results (Fig. 3, Table I). Fig. 4 illustrates the diversity of such large grain origins ranging from thin platelet grains (Fig. 4A and B), tabular grains (more commonly with transgranular fracture, Fig. 4c), approximate spherulitic grain clusters (Fig. 4c), frequently associated porosity (Fig. 4d and e) and relatively equiaxed grains (Fig. 4e–g). Using the size of grain cluster origins for C in Equation 1 gave approximately the polycrystalline K_{IC} thus showing that the largest G of such clusters was substantially $< C$.

Kirchner and co-workers [23, 24] showed of 20 hot-pressed Al_2O_3(+ 1/4% MgO) and 20 sintered specimens (of the same 96% commercial Al_2O_3 body

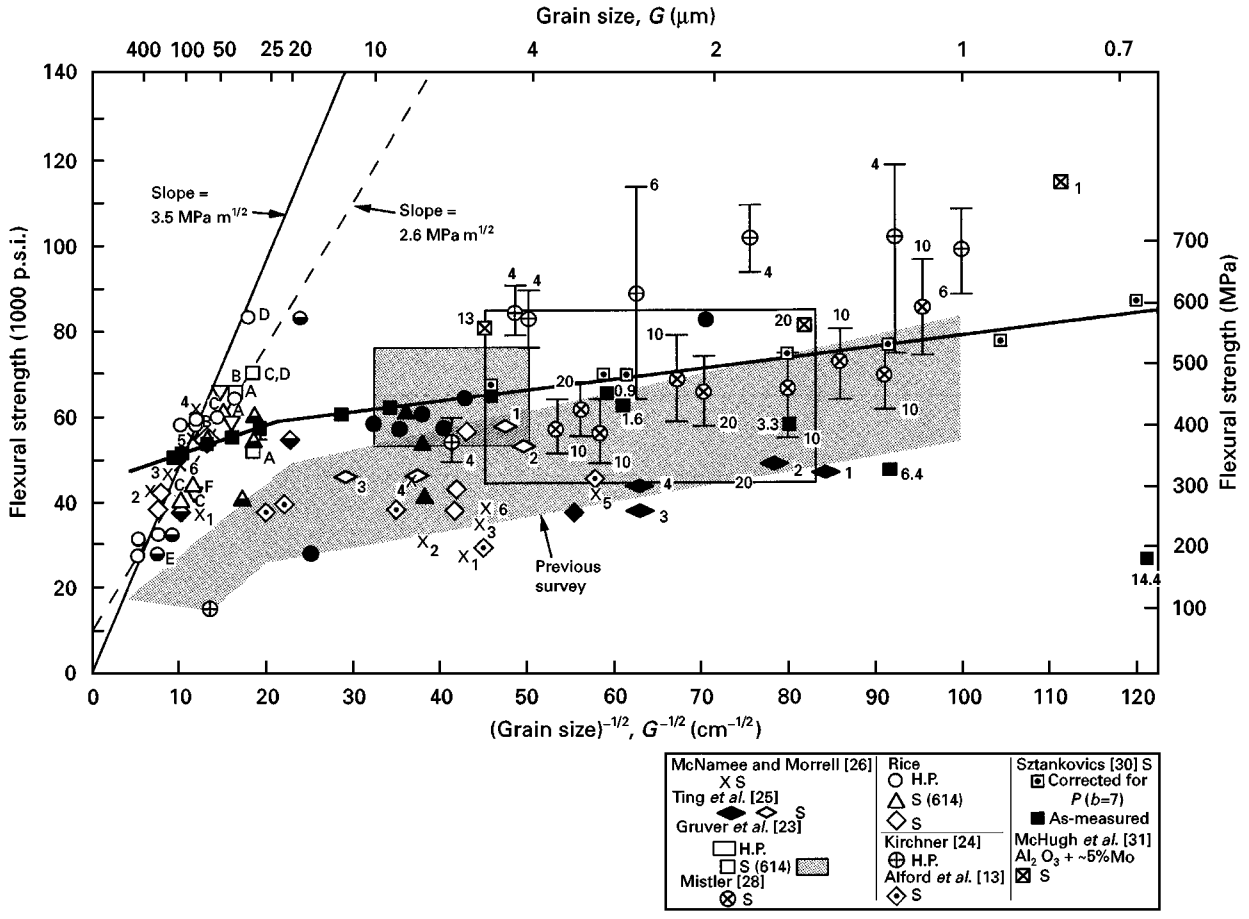

Figure 3 Further σ–$G^{-1/2}$ data for machined Al_2O_3 at 22 °C. Present data for hot-pressed and sintered 96% and 99% Al_2O_3 shown by fractography to have failed from large isolated or clustered grains (e.g. Fig. 4a–e). Solid symbols, G_a, open symbols, individual G or cluster size at origin; half-filled symbols $= G_m$ in a grain cluster from which failure originated. Also shown are data of (1) Gruver *et al.* [23] for hot-pressed (HP) and a commercial 96% sintered (S) Al_2O_3 (respectively, right and left-hand boxes showing σ and G_a ranges, open symbols for specimens failing from large grains); (2) Ting *et al.* [25] (99% + Al_2O_3 and McNamee and Morrell [26] (95% Al_2O_3) versus G_a and G_m values obtained from their microstructural (not fractographic) examinations (numbers next to points to identify points versus G_a with no P correction, and versus G_m with P correction, respectively 0.5%–2.5% with $b = 8$ and 3.5%–5.1% with $b = 6$, as per the Appendix); (3) hot-pressed data of Kirchner [24] and Gruver *et al.* [23] and sintered data of Mistler [28] (verticle bars are standard deviation; associated numbers are the number of tests) and Gruszka *et al.* [29] (both for 99.5% Al_2O_3 substrates), Sztankovics [30] (shown without and with P ($\geqslant$ 0.5–1.4%), correction with $b = 7$ as per the Appendix, numbers with a decimal point are the per cent porosity); (4) the range of data using G_a from a previous survey [3] (shaded area), all versus G_a; and (5) McHugh *et al.* [31] (Al_2O_3 + 0%–5.5% Mo).

used by the present author), respectively, 2 and 7 failed from (mainly single) large grains (Fig. 6) (such origins from single large grains, in contrast to those of the present author commonly from clusters of larger grains or large grains and associated large pores, is attributed to material variability and processing differences, illustrating the danger of arbitrarily using G_m. Earlier studies of this author on this material showed a higher incidence of failure associated with larger grains, which was a major factor in noting the importance of large grains as fracture origins [3]. However, subsequently different lots and times of manufacture as well as different part sizes and substantially more samples showed only 7% of 155 failures occurred from large grains – 36% from isolated pores, 16% from flaws at bar corners, 30% from probable tensile surface machining flaws and 10% not identified. Further, this authors specimens were machined from cold-pressed discs of substantial size ($\geq$ 5 cm diameters), whereas the specimens of Gruver *et al.* [22] were extruded ($\sim$ 3.2 mm diameter) rods. The smaller size and especially the high shear in extrusion as well as the absence of spray drying and associated porosity, provide excellent opportunities for reducing larger defects, e.g. larger agglomerates often giving larger grain clusters in the resultant sintered bodies. Their data, plotted versus G_a or G_m, agree with the current data and a previous survey [3] (Fig. 3). Again, the primary effect of plotting specimens failing from larger grains versus G_m is to move a fraction of the data points (mostly from the lower half of the σ range) significantly to the left. This increases the slope of the large G branch, but it is still less than the polycrystalline K_{IC} (Table I), and indicates a σ intercept of > 0 at $G = \infty$. The frequent transgranular character of many large G origins (and often in the surrounding area) argue against bridging, which commonly involves intergranular fracture [19].

Gruver *et al.* [23] showed similar 96% Al_2O_3 origins from isolated large grains over a range of temperatures. Using half these G_m values as C for the large grain (of 20) fracture origins in liquid nitrogen gave

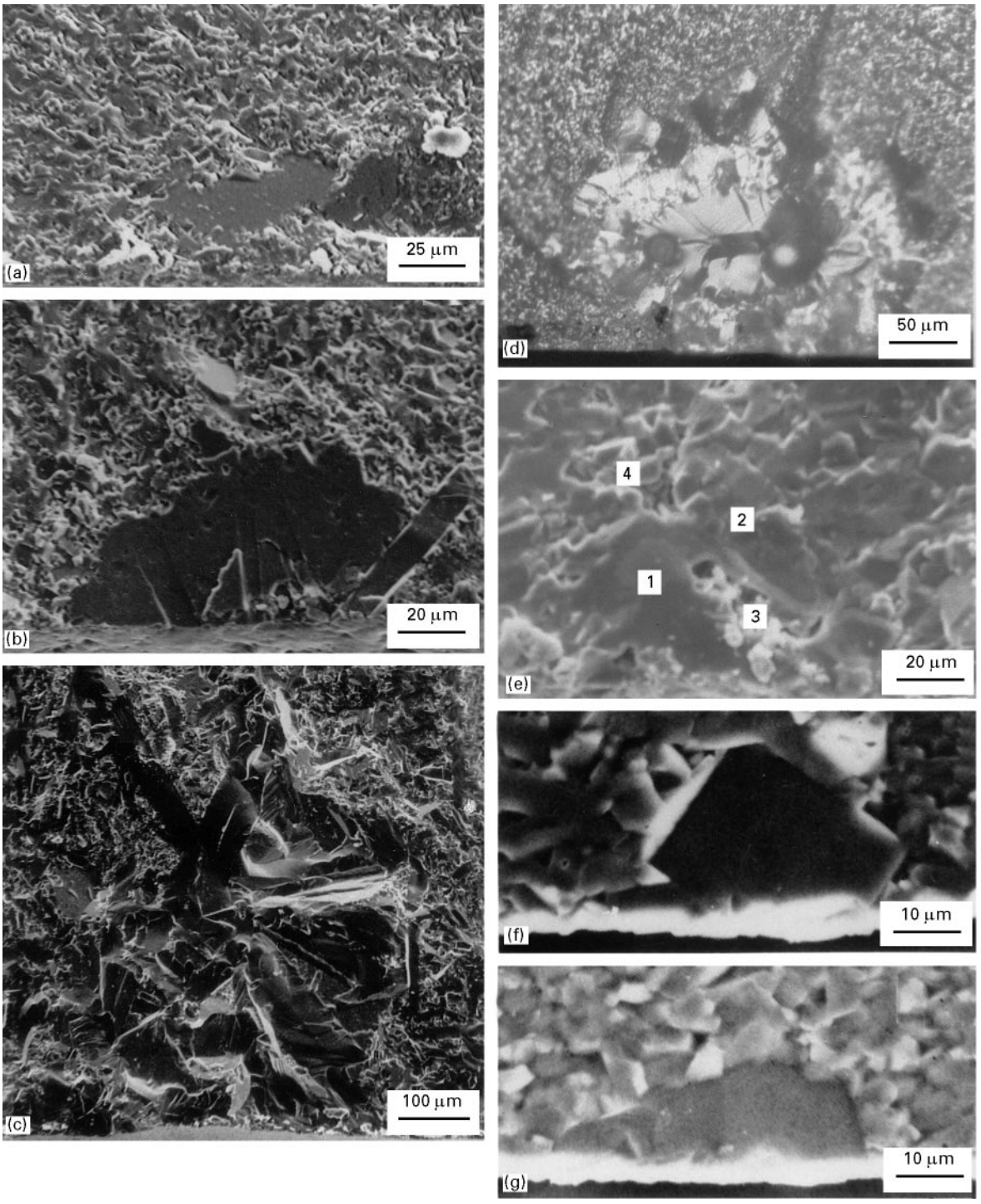

Figure 4 Examples of Al_2O_3 failures from isolated large grains or grain clusters. (a–c) Hot-pressed Al_2O_3 of this study. Note failure (a) between a large (probably thin, platy) grain and the abutting finer grain structure (which also contained three additional tabular grains), plus one tabular (transgranularly fractured) grain ($\sigma = 583$ MPa); (b) a collection of three platy grains (the one furthest to the right was confirmed by higher magnification and other orientations to be a thin, platy grain $\sigma = 405$ MPa); (c) an approximately circular cluster of tabular grains (all transgranularly fractured, $\sigma = 319$ MPa); (d) a large (transgranularly fractured) grain with two pores and surrounding larger grains (optical micrograph of 99% sintered Al_2O_3, $\sigma = 291$ MPa); (e) two larger grains (1, 2) and two (3, 4) pores in a sintered, 96% Al_2O_3, $\sigma = 423$ MPa; (f), (g) large grain-fracture origins in the commercial 96% Al_2O_3 specimens of Gruver *et al.* [19], (f) at 22 °C, $\sigma = 376$ MPa, and (g) at -196 °C, $\sigma = 593$ MPa.

K_{IC} 3.9 ± 0.6 MPam$^{1/2}$, and 7 of 20 in the 95% (and 2 of 20 hot-pressed) Al_2O_3 having large grain origins at 22 °C gave K_{IC} 3.2 ± 0.3 MPa$^{1/2}$. While these all generally agree with the polycrystalline K_{IC}, all gave at least one value more or equal to two standard deviations below the average, suggesting that in those cases the grains were not the complete flaw, i.e. C extended into the surrounding average grain structure, so plotting σ value for those G_m values is questionable. Similarly, it cannot be ruled out that large grains giving the highest calculated K_{IC} values may have resulted in failure before the flaw reached the full grain size, i.e. the critical flaw size was $< G$.

Sintered, machined Al_2O_3 data of Ting *et al.* (99 + %) [25] and McNamee and Morell (95%) [26] versus G_m (from microstructural, not fractographic

studies) are, respectively, simply moved leftward in the finer G regime and from the finer to the larger G branch compared to the use of G_a. In either case their data agree with the other data shown (especially when corrected for P, (respectively, 0.5%–2.5% and 3.5%–5.1% using $b = 8$ and 6, see Appendix) Fig. 3), as does Alford *et al.* [13] (99 + %) machined data compared with G_m (the only values given). Sztankovics' larger G_a data are consistent with G_m plotting for failure from isolated large grains or grain clusters in the present study. Finer G data for machined Al_2O_3 of Kirchner *et al.* (hot-pressed) [23, 24], Al_2O_3 of Mistler [28] and Gruszka *et al.* [29] (sintered, 99.5% substrates with 0.5% MgO and 2%–3% porosity), Sztankovics [30] σ (sintered, corrected for $P =$ 0%–14% with $b = 7$, Appendix), and of McHugh *et al.* [31] (Al_2O_3 + 4.3%–5.5% Mo, one sample with no Mo at $\sigma = 255$ MPa, $G_a \sim 50$, is just to the right of the larger G branch, see also Fig. 5), all versus G_a, also generally agree with one another and other Al_2O_3 data [3], and clearly show a > 0 finer G slope. Higher σ values, especially at finer G, are attributed to use of MgO and limited, fine P, and the use of small, polished, extruded rods or tape cast substrates with possible preferred orientation [28, 29] all indicate reasonably homogeneous G (e.g. only two of Kirchner *et al.*'s samples indicate larger G values by their progressively lower σ values). Recent substantial data of Tomaszewski [32] agree very well with the earlier Al_2O_3 survey [3], i.e. they are the mean of the survey range, with larger and finer G branch slopes of 2 and ~ 0.6 MPam$^{1/2}$, respectively, and a probable $\sigma < 0$ intercept at $G = \infty$.

Now, let us consider Al_2O_3 tested with as-fired surfaces. Charles' data [33] for larger, ~ 1.7 mm diameter, extruded (lamp envelop quality Al_2O_3) rods versus G_a (including the large G values, in the next to the largest G body found to have essentially a bimodal microstructure, Fig. 5), (1) lie at, or a limited distance to the left of, the upper limits of a previous survey [3] and other machined Al_2O_3 (Figs 2 and 3), and (2) show a substantial finer G slope. Data for smaller (< 1 mm diameter) extruded, sintered Al_2O_3 rods of Blakelock *et al.* [34] and Bailey and Barker [35] versus G_a show similar slopes which are also supported by these data extrapolating to σ–$G^{-1/2}$ values for Al_2O_3-based fibres [7, 36–40]. Alford *et al.*'s [13] data versus G_m are better fit by a positive, rather than their proposed zero, finer G slope. (Specifics of their G_m measurement were not given other than noting that G_m values were typically 2 to 3 times G_a. The one fractograph they showed indicated fracture from a cluster of three larger grains.)

Al_2O_3 with limited molybdenum [31, 41], tungsten [42] or ZrO_2 [43] additions which inhibit grain growth (especially the occurrence of exaggerated grains) versus G_a generally agree (whether machined or as-fired) with the preceding data and trends (Fig. 6, Table I). These data trends are also consistent with

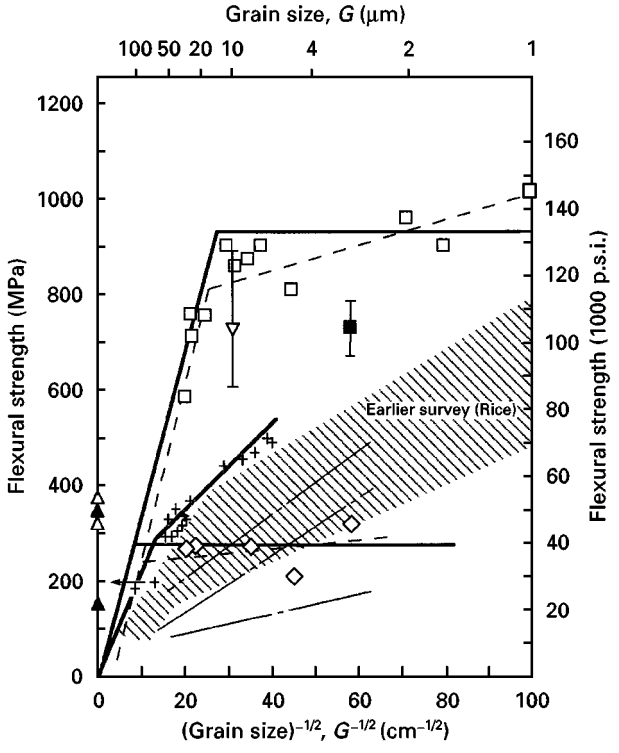

Figure 5 (△, ▲) Al_2O_3 σ–$G^{-1/2}$ data at 22 °C for as-fired specimens. Charles [33] (+ − +) larger extruded rods of lamp envelope material σ versus G_a (arrow reflects the larger G of a bimodal G in one set of samples). Heavy lines (—) through Alford *et al.*'s [13] data for small extruded rods reflects their data presentation (versus G_m) (– – –). An example of alternate fitting of the data. Data are also given for small extruded and fired rods of (–■–) Blakelock *et al.* [33] and (▽) Bailey and Barker [34] (lines are for more porous bodies, individual points for denser bodies) versus G_a. Also shown are Alford *et al.*'s lower σ, (□, ◇) die-pressed and machined Al_2O_3 (see also Fig. 3).

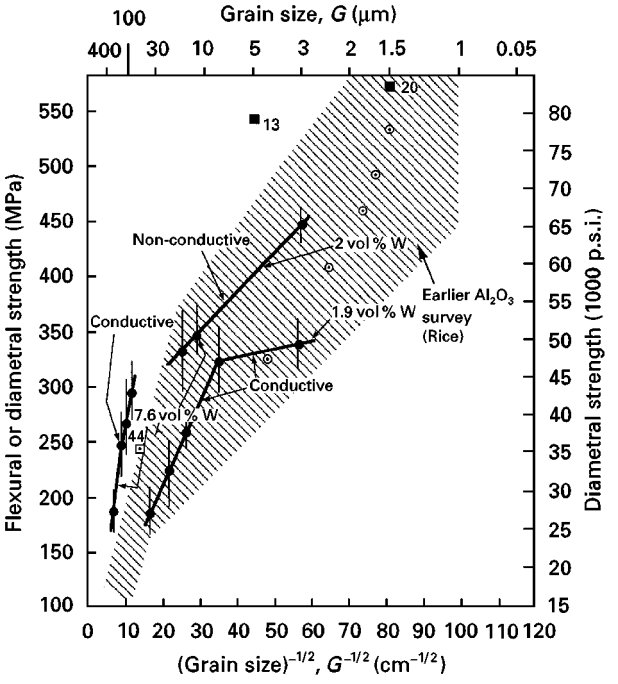

Figure 6 Al_2O_3 + W [42], Mo [31, 41] or ZrO_2 σ–$G^{-1/2}$ data at 22 °C versus G_a. (◖) Flexural data of (●) Hing [42] for isopressed, as-fired rods of Al_2O_3 plus 1.9–7.6 Vol% W, with the presence or absence of contiguity of the tungsten particles indicated by their electrical conductivity. All but the highest σ sample of Hugh *et al.* [31] for Al_2O_3 + 4.5%–5.5% Mo are shown (see also Fig. 3): (■) Al_2O_3 + 4.3% − 5.5% Mo, (⊡) Al_2O_3. (⊙) Al_2O_3, 1% − 5% ⩾ ZrO_2 (Hori *et al.* [43]).

σ–$G^{-1/2}$ trends from diameterical strengths of Al_2O_3 + Mo [44, 45] and hot-pressed Al_2O_3 [3] which also showed positive finer G slopes, and possible $\sigma > 0$ intercepts for the larger G branch.

3.2. B_4C, β-Al_2O_3, TiO_2, Y_2O_3 and SiC data

A plot of σ versus G_m at B_4C fracture origins from an earlier survey [3] and this study generally agrees with the previous study [3] based on G_a, but would extend the large G branch somewhat leftward and increase its slope (Fig. 7). More detailed fractography shows why some of the data points are (incorrectly) moved further to the left than most of the data, and some not far enough by using G_m. Thus, (1) in Fig. 8, the origin is from the smaller of the two large grains and the small pore they abut (because single-crystal mist occurs within the larger grain and mist commences at $\sim 10C$ [18, 19] and using the smaller grain as C yields $K_{IC} \sim 3.4$ MPam$^{1/2}$, (2) a machining flaw (Fig. 9), by itself too small by a substantial margin to be C, but combining this flaw and the two large grains and the intervening material between, is not (i.e. giving $K_{IC} \sim 3.4$ MPam$^{1/2}$ from equation 1), (3) a corner origin with a substantial number of large grains (~ 100 fold larger than G_a, generally highly twinned, Fig. 10) gives $< 1/2$ the K_{IC} for B_4C using the large $G/2$ as C, indicating that C probably encompassed more than one of these large grains, (4) correcting for the substantial internal nature of the origin (reducing σ by $\sim 15\%$) gives a high K_{IC} value using the very large grain as C (Fig. 11), suggesting that failure occurred before the flaw reached the boundaries of this large grain, and (5) failure from a flaw (from maching parallel with the tensile axis) despite there being at least three substantially larger grains in the vicinity, one of

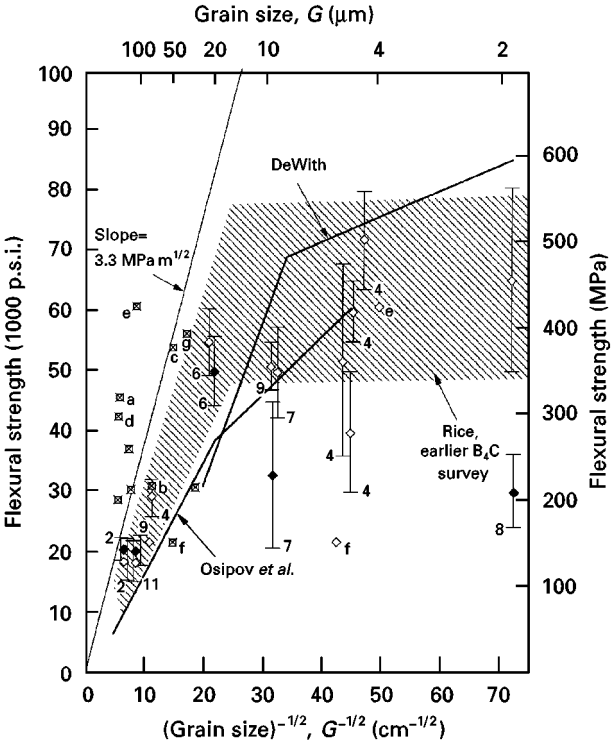

Figure 7 B_4C σ–$G^{-1/2}$ data at 22 °C. Hot-pressed specimens of this study ground (◇) parallel or (◆) perpendicular to the tensile axis plotted versus G_a (vertical bars and associated numbers are the standard deviation and number of tests). Some of these, and earlier specimens of this author are also shown (☒) versus G_m from fractography (e.g. Figs 11–16). Also shown are a range of data from an earlier survey [3] (versus G_a, crosshatched region) and the average (hot-pressed) data trends of Osipov *et al.* [41] and DeWith [42] versus their G_a.

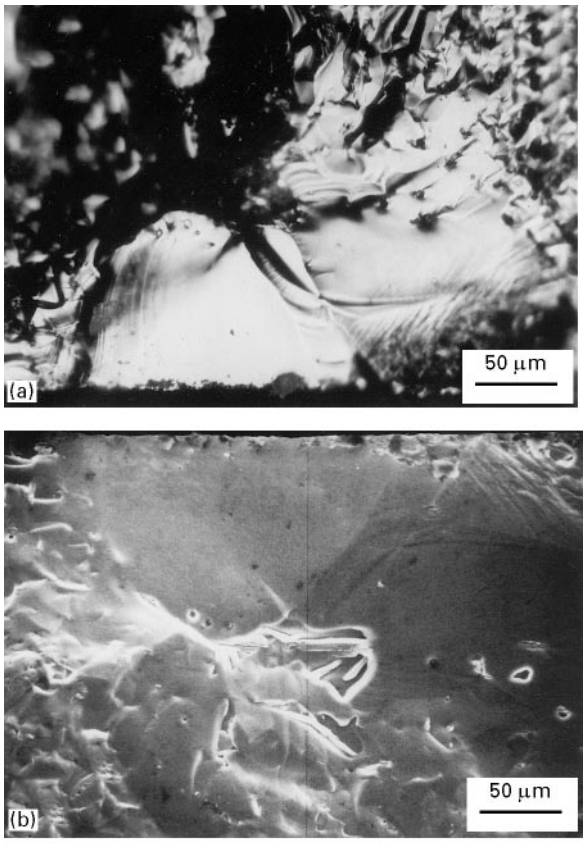

Figure 8 B_4C failure from an internal pore and a larger surface grain. (a) Optical micrograph and (b) scanning electron micrograph of the origin showing failure initiated from the pore at the junction of the two large grains, propagating downwards towards the tensile surface and right into the adjacent large grain (single crystal mist and hackle features show that the fracture had reached criticality when it entered the right grain, [18, 19]. The sample (ground parallel, point d of Fig. 9) failed at 298 MPa (42.7×10^3 p.s.i.).

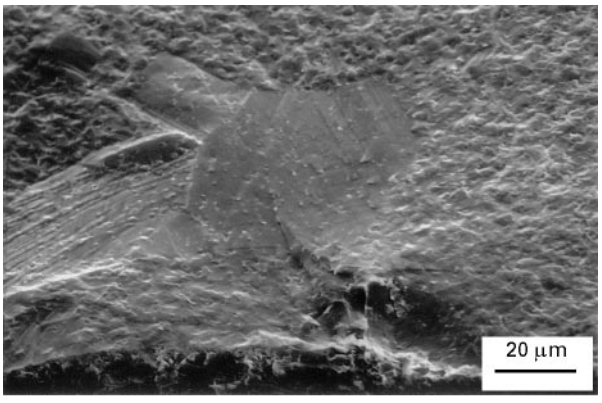

Figure 9 B_4C initiation from a machining flaw and nearby larger grains. The machining flaw (bottom right of centre) is not nearly large enough to be the origin of failure at MPA (54.2×10^3 p.s.i.), but a flaw encompassing the machining flaw plus the two large grains above and to the left of the machining flaw is (point c of Fig. 9).

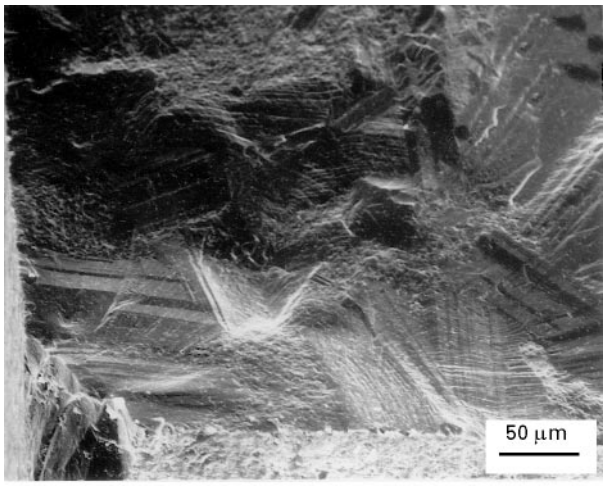

Figure 10 Failure initiation from machining damage at the corner of a B_4C sample having a number of large grains (nearly 100 times the finer grain structure of the rest of the body). Note also the striations on these large grains indicating substantial twinning. Failure initiation at 215 MPa (30.8×10^3 p.s.i.) (point b of Fig. 9) shows the flaw size most likely encompassed more than one of these large grains.

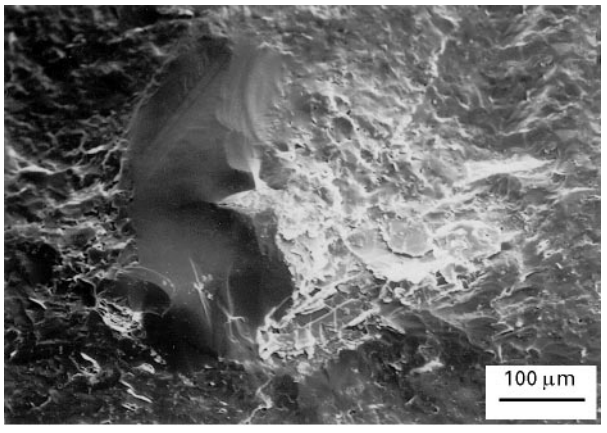

Figure 11 Failure from a large, internal grain in B_4C and porous area (to the right of the grain). Failure stress at the tensile surface was 350 MPa (50×10^3 p.s.i), point a in Fig. 9), but at the grain centre (about 1/6th of the distance to the neutral axis) was about 280 MPa indicating C was less than or equal to the large grain size.

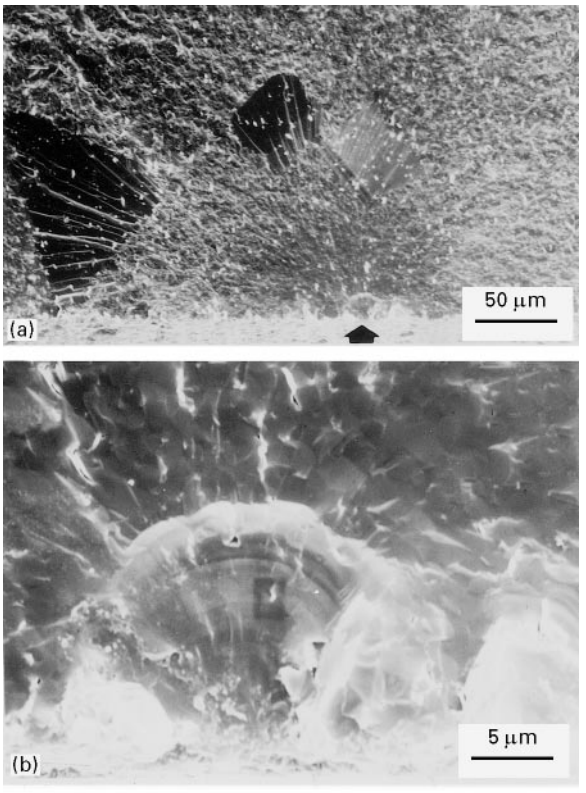

Figure 12 Failure initiation in a B_4C sample not occurring from available large grains. (a) Lower magnification showing the fracture origin (arrow) and the surrounding fracture region containing at least three much larger than average grains. (b) Higher magnification of the actual failure origin from a machining flaw (consistent with its failure stress of 427 MPa, 61×10^3 p.s.i.), point C in Fig. 7.

which is also connected to the tensile surface (Fig. 12). Plotting the strength of this latter specimen versus G_m in the vicinity of the origin clearly puts the data point far to the left of the slope of the other data. Although samples of failure initiation not occuring from large grains were not previously sought by this author or other investigators, Fig. 12 shows unequivocally that this can indeed happen. Thus, the arbitrary use of G_m even in the vicinity of the fracture origin can lead to serious errors. Similarly, fractographic examination of the lowest σ data point in Fig. 7 shows that while there is considerable grain heterogeneity in this sample, failure initiation was from an unusually elongated flaw (actually a series of individual flaws) from machining perpendicular to the tensile axis and that again none of the large grains present determined the failure σ. The fractographically based B_4C data give the larger G branch slope as being $\leqslant K_{IC}$ (Table I) with a $\sigma = 0$ intercept. Note, (1) extensive transgranular fracture and mist and hackle (Figs 8–11) arguing against significant bridging, which typically is via mostly intergranular fracture, and (2) the common occurrence of twinning in B_4C (e.g. Fig. 10) may be a factor in the less possible effect of large grains being fracture origins and 100% transgranular fracture in B_4C (from $G \sim 1$ to > 100 μm), compared with 0 to $\sim 50\%$ in Al_2O_3 [4, 18] due to stress relief. Finally, while probable effects of larger grains would shift much of Osipov *et al.* [46] and DeWith's [47] more recent σ versus $G_a^{-1/2}$ data leftward with the other B_4C data (Fig. 7), their data should still indicate positive slopes for the finer G branches.

Data for (mostly hot-pressed) β''-Al_2O_3 bodies of Virkar and Gordon [48] versus G_m (G_a values and specifics of the G_m determination were not given), clearly showed the larger G slope $< K_{IC}$ (Table I), and the finer G slope probably > 0 (Fig. 13). More limited earlier data for (1) hot-pressed β'' of Virkar *et al.* [49] and β of McDonough *et al.* [50] (where fractography showed no unusually large grains at the fracture origins), (2) HIPed $\beta + \beta''$ of May *et al.* [51] and (3) sintered samples of (a) Stevens *et al.* [52] (β, correction for $P \sim 2\%$ would increase σ by $\sim 5\%$–10%), (b) Lingscheit *et al.* [53] (β'', correction for $P = 1.5\%$–4% would increase σ by $\sim 4\%$–9% at the lower porosity level and 11%–21% at the higher porosity level, and (c) Francis *et al.* (β, corrected for $P = 3\%$–9.5% using $b = 8$ at the two finer G's, $b = 4$ at the largest G and

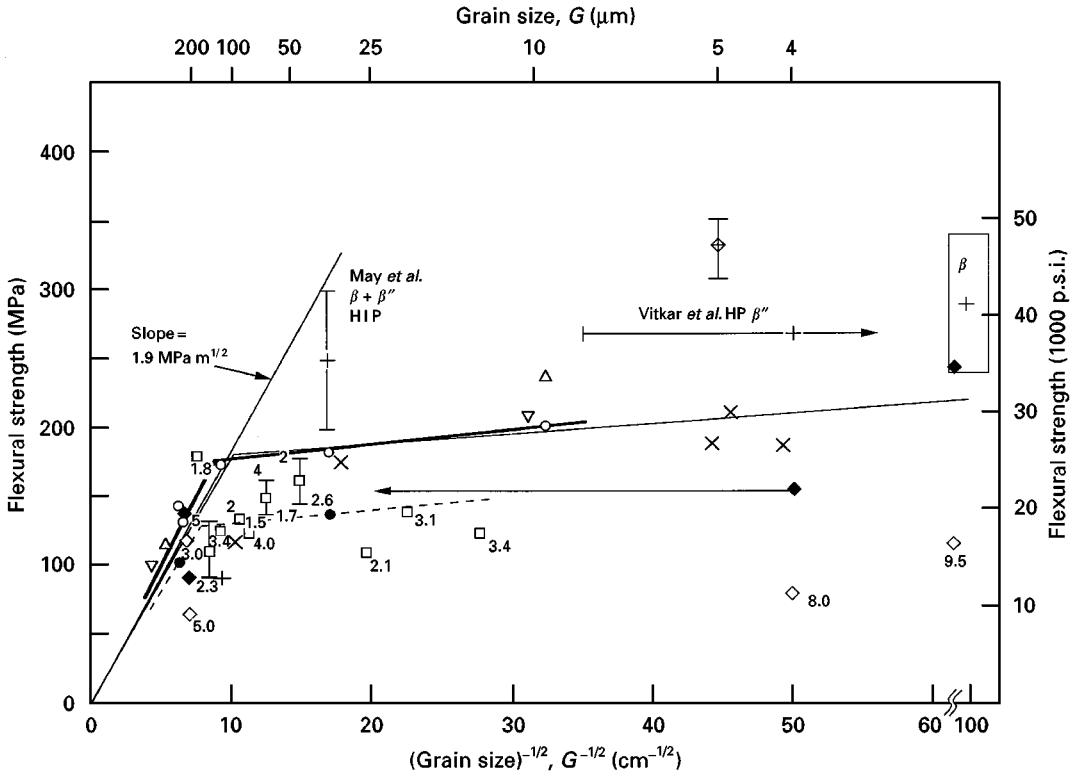

Figure 13 σ–$G^{-1/2}$ at 22 °C for various β-alumina bodies. (○, ▽, ●, △, +, ×). Data from Virkar and Gordon [48] for (mostly) hot-pressed β″ (composition and processing: 8.8% Na_2O–0.75% Li_2O, HP, (○) mode A, (▽) mode A′, (●) mode C, (×) S (zeta process). (△) 8.6% Na_2O–0.70% Li_2O, HP, mode A. (+) 8.9% Na_2O–0.70% Li_2O, S.), plus earlier, similar material of Virkar *et al.* [49], HIPed mixed β + β″ of May *et al.* [51], (◆), hot– pressed β of McDonough *et al.* [50] and sintered data of Stevens (β) [52]. (range shown by box), (□) Lingscheit *et al.* (β″) [53] and (◇, ◆) Francis *et al.* (β) [54]. Vertical bars: May *et al.*'s data range [51], Lingscheit *et al.*'s [53] standard deviations, whole number superscripts indicate the number of specimens averaged, subscripts with decimal points for Lingscheit *et al.* and Francis *et al.* are the percentage *P*. Solid data points for Francis *et al.* show the strengths corrected to $P = 0$, all data versus G_a, except Virkar and Gordon (versus G_m). The arrow for the *G* range for Virkar *et al.* [49], and the arrow for one datum point of Francis *et al.* shows the *G* range.

$b = 6$ at the intermediate *G*, see Appendix) all versus G_a are reasonably consistent with one another and Virkar and Gordon's data, especially when corrected for porosity. The second finest *G* body of Francis *et al.* had isolated tabular grains. Using these as *G* would move this data point substantially to the left but not to the large *G* branch, thus indicating they were not large enough to equal *C*. Collectively, they clearly indicate a positive slope for the finer *G* branch(es), a larger *G* branch slope $< K_{IC}$, and uncertainty in the σ intercept at $G = \infty$.

Machined TiO_2 data of Kirchner and Gruver's [55] (hot-pressed, $P \leqslant 3\%$) versus G_a, Alford *et al.*'s [13] (lower σ specimens from sintered, die-pressed discs) are reasonably consistent regardless of whether G_a or G_m are used for Alford *et al.*'s data (Fig. 14). Alford *et al.*'s small (< 1 mm diameter) as-fired extruded rods, with expected higher σ have the larger *G* slope $< K_{IC}$ (when it is recognized that $C = G/2$, not *G* as they used [13], and the zero σ intercept at $G = \infty$, and finer *G* slopes $= 0$ are quite uncertain, and not supported by Kirchner and Gruver's data.

Cappola and Bradt [56], Rice [5], and Seshadri *et al.* [57] (sintered α, $P \sim 1.6\%$), SiC data based on G_a, generally agree (Fig. 15), as do those of Cranmer *et al.* [10] (using G_m). Gulden's [58] CVD SiC data ($0.6 \pm 0.5\%$P), based on G_a are also consistent, recognizing the higher σ due to use of small, polished specimens, and supports a positive fine *G* slope, as does Cranmer *et al.* [10]. Prochaska and Charles [11] plotted σ (< 140 to ~ 350 MPa) versus the length *L* of the large tabular (exaggerated) α-grains at fracture origins in the β-SiC matrix, obtaining a slope of 3.9 $MPam^{1/2}$ with a $G = \infty$ intercept at ~ 70, not 0, MPa). However, such use of the maximum grain dimension, *L*, is not correct, because it violates $C = G/2$ as well as other fracture mechanics criteria (discussed later). Use of a *G* value based on the equivalent circular area (assuming the grain width $\sim L/10$, from their micrographs) lowers the slope to ~ 2.3 $MPam^{1/2}$, more consistent with the other data. Tekeda and Nakamura's [59] SiC (using 1%–2% levels of different additives, including *C* to affect *G*, as did some others [10, 11]) σ plotted versus G_a and G_m (measurement specifics not given) lies to the right of the other data (Fig. 15). However, the G_m values (from general microstructural examination) are likely to be $< G_m$ at fracture origins (not determined), especially at medium and larger *G*. Correction for this would likely bring their data into agreement with the other SiC. Larsen *et al.*'s [60] SiC σ's versus measured G_m, as well as variable G_a values for various SiC materials (Fig. 16) are consistent with Fig. 15 and the model of Fig. 1 based on their fractography. This showed most higher σ failures occurred from undetermined origins (i.e. no dominant features such as large grains in the origin

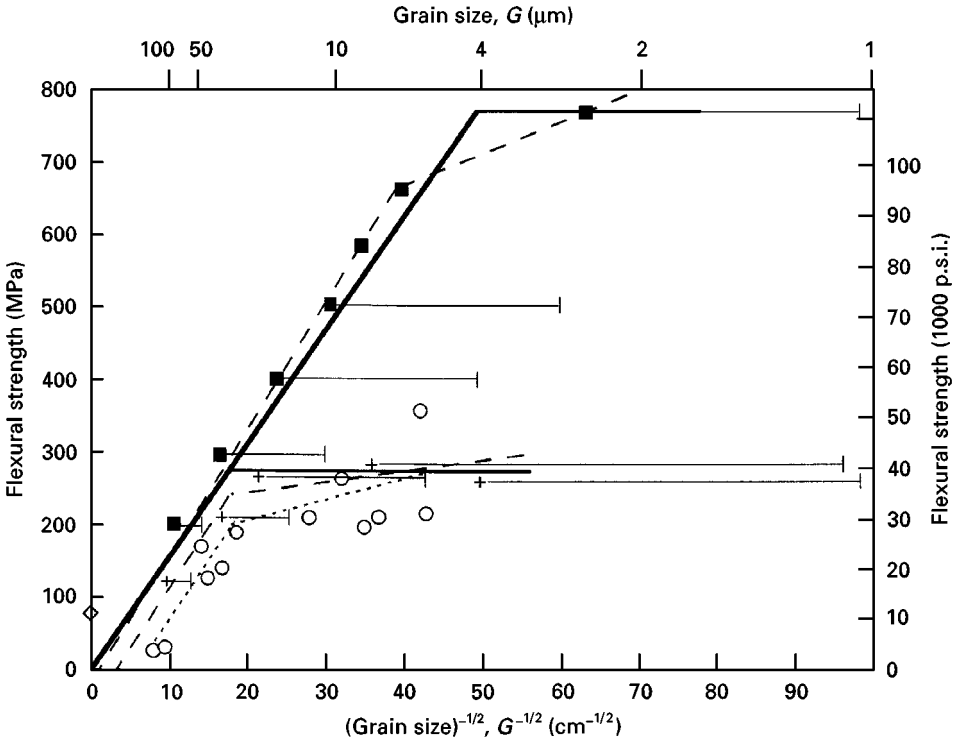

Figure 14 (◇) TiO_2 σ–$G^{-1/2}$ data at 22 °C. Data for (1) machined bars cut from hot-pressed discs of (--○--) Kirchner and Gruver [55] and from (■, VP; (+, PP)) die-pressed and sintered discs of Alford *et al.* [13]. Data are shown as a function of G_a but the data of Alford *et al.* are also shown versus G_m (horizontal bars). (——) Alford *et al.*'s presentation; (– – –) alternatives suggested in this study.

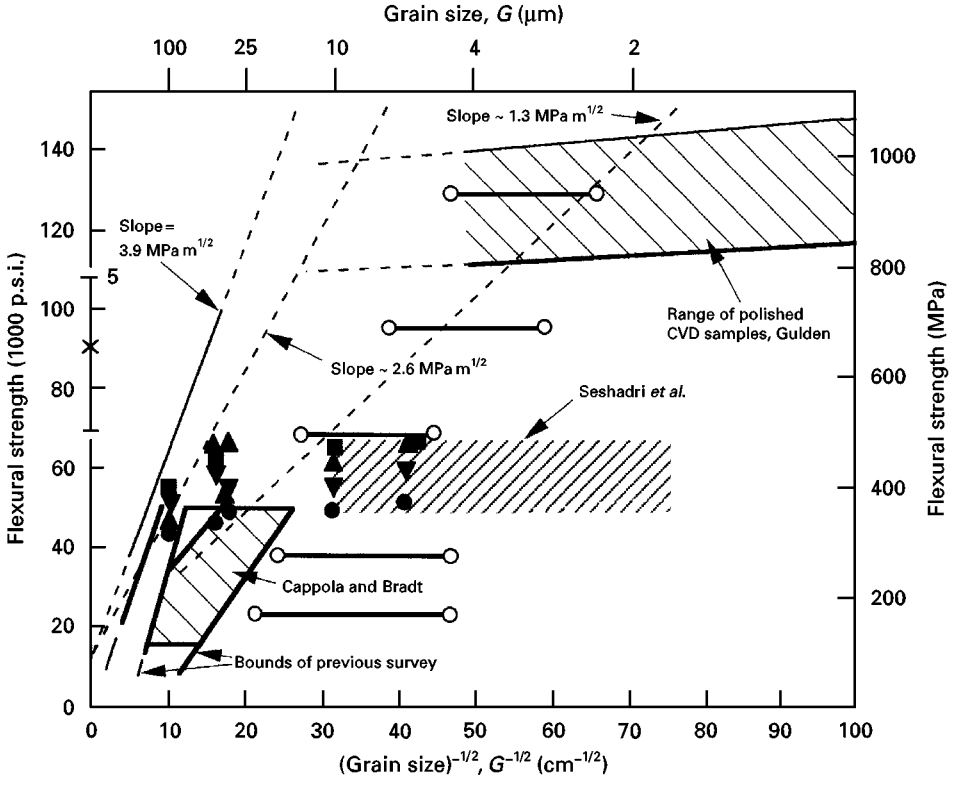

Figure 15 SiC $\sigma - G^{-1/2}$ data at 22 °C. Data of Capolla and Bradt [56], Rice [3], Gulden [58] (polished CVD specimens, $P = 0$ to 1%) and Seshadri *et al.* [57] (sintered α, $P = 1.6\%$) plotted vs. G_a and that of Cranmer *et al.* [10] (ground perpendicular to the 'tensile axis with grits shown), Tekeda and Nakamura [59] (hot pressed, $P = 0$–3%) vs. G_a and G_m. The range of Prochazka and Charles [11] data for their dense sintered β-SiC is shown by the solid section on the line with a 3.9 MPam$^{1/2}$ slope, based on their use of the maximum dimension of the isolated large tabular α grains from which these specimens failed. The dashed line (slope ~ 1.3 MPam$^{1/2}$) represents an approximation for the width of these grains. The intermediate dashed line (slope ~ 2.6 MPam$^{1/2}$) for G_a (based on equivalent circular area of the grain), agrees much better with the other data. (Slopes are calculated using the grain dimensions as the flaw size; i.e., need to be multiplied by 0.71 to give K_{IC}).

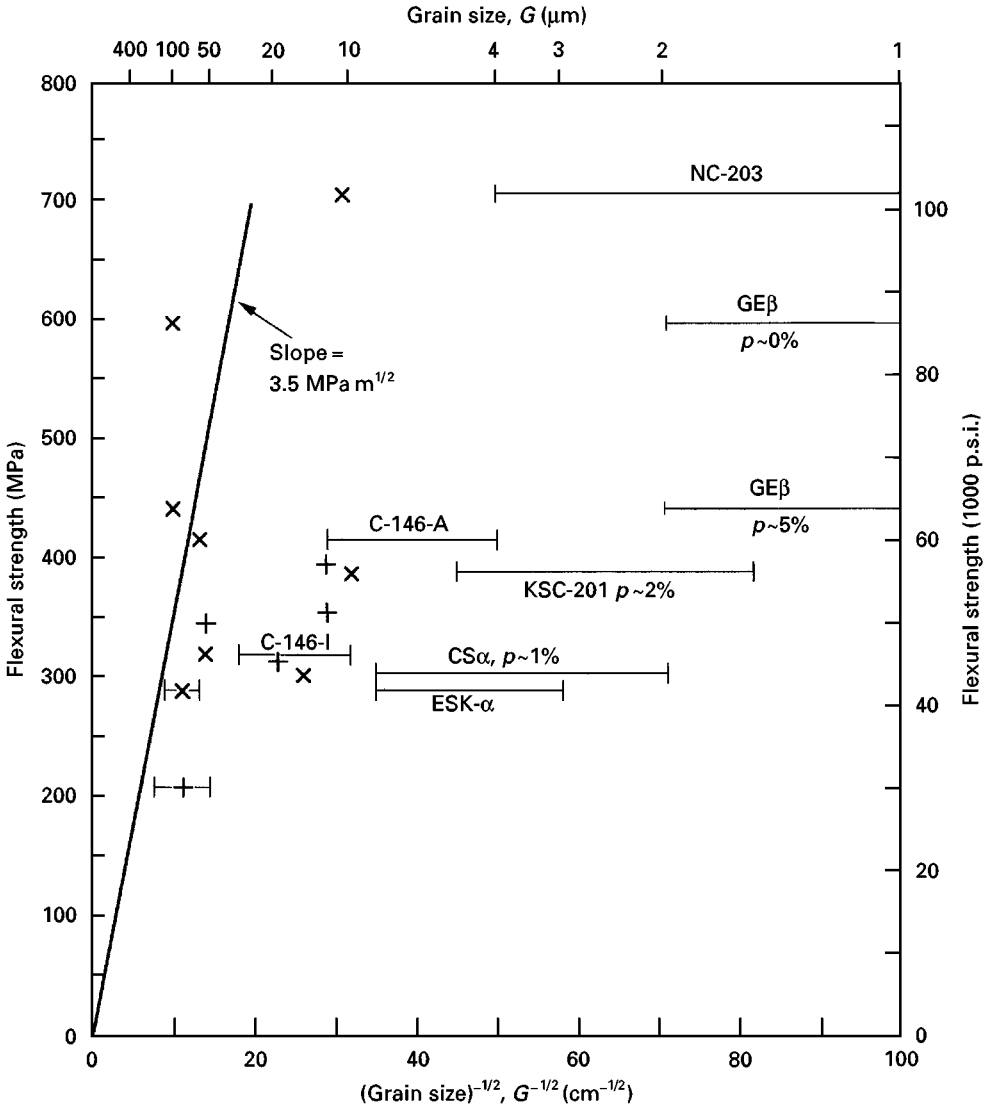

Figure 16 Larsen *et al.*'s [60] SiC data at 22 °C. Data plotted vs. the G_m agrees with a slope of $\leqslant K_{IC}$ (i.e., $\sim 0.71 \times 3.5$ MPam$^{1/2}$), and data plotted vs. variable G_a (horizontal bars to the right) are consistent with such points being on finer G branches (Fig. 1). Note both hot pressed and sintered data represented (porosity of the latter is indicated, and in the more extreme cases (for GE β corrected to $P = 0$ as indicated, using $b = 6$, see Appendix).

area), thus being more consistent with G_a values, and hence being on finer G branches (of which there should be more than one, substantial scatter, or both, in view of different and varying flaw populations), while lower σ's (e.g. < 450 MPa) showed failure from various flaws. Recognizing G_m values are tabular grain lengths (e.g. in the GE (General Electric) β material) hence excessive for the appropriate G_m value (as discussed later), shows the larger G slope is $< K_{IC}$ (~ 3.5 MPam$^{1/2}$). Plots for Larsen *et al.*'s [60] hot-pressed and reaction-sintered Si_3N_4 (corrected to zero porosity, see Appendix, Fig. 17) show the same trends, i.e. (1) at finer G, higher σ's from machining flaws rather than microstructural heterogeneities, and lower σ's from microstructural heterogeneities such as large tabular grains, and (2) the larger G slope (using G_m) is $< K_{IC}$ ($\geqslant 4$ MPam$^{1/2}$, for $P = 0$).

It is useful to contrast the above materials, which are non-cubic, or have non-cubic phases, exhibiting exaggerated grain growth, with cubic materials. Cubic materials show the same σ–$G^{-1/2}$ trends as Al_2O_3, BeO, TiO_2, B_4C and SiC; i.e. the values of σ for many larger G as less than those for single crystals, larger G branch slopes are less than K_{IC}, larger G–finer G branch intersections at $C \sim G/2$, and finer G branch slopes > 0 [3–7]. However, of the two cubic materials for which there are most data, limited fractography data for ZrO_2 [18], and more for $MgAl_2O_4$ [5] provides no evidence of G_m controlling σ, but support the use of G_a. Extensive fractography of dense, hot-extruded (textured) MgO, whether σ was controlled by slip–crack nucleation or flaws, also showed no evidence of G_m controlling σ, and in fact supports the use of an average G [61]. Although significant σ–$G^{-1/2}$ data for dense Y_2O_3 are not available, σ and fractography of large G (transparent) specimens reveals machining flaws, generally too small relative to G to grow to the size of G before failure [62]. This shows no support for G_m determining σ, and again support use of an average G (Fig. 18a–d). These also illustrate many of the problems of using G_m in large G bodies, i.e. failure from (1) a surface grain, much of which has been removed by machining (Fig. 18c), (2) one or more smaller surface grains with machining

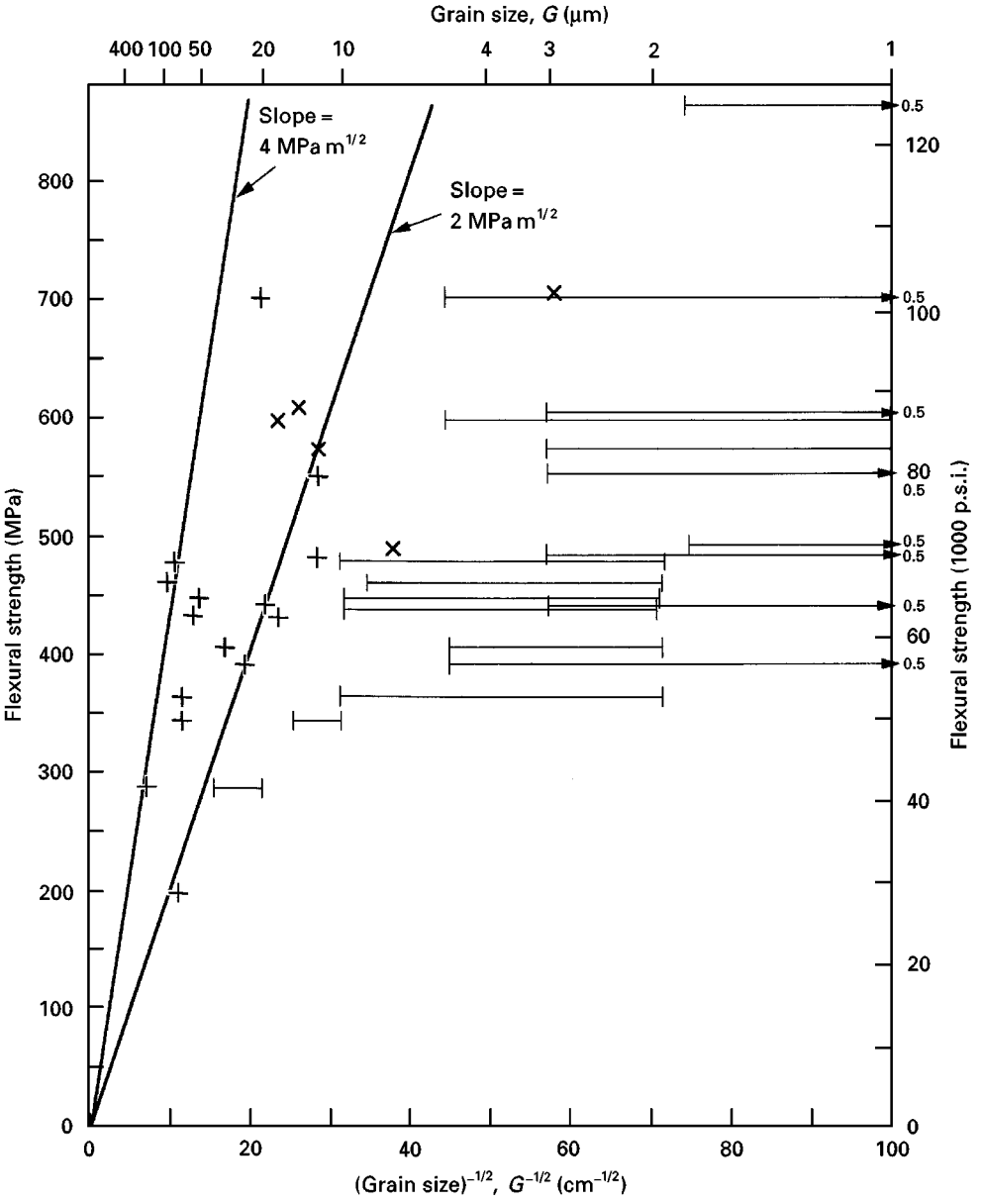

Figure 17 Larsen *et al.*'s [60] Si_3N_4 data at 22 °C. Data plotted vs. G_m agrees with a slope $\leqslant K_{IC}$ (i.e., 0.71×4 MPam $^{1/2}$), while data plotted vs. G_a (horizontal bars to the right) is consistent with such points being on finer G branches (Fig. 1). Hot pressed and RSSN data plotted (the latter corrected to $P = 0$ using $b = 4$, see Appendix), most corrections are $\leqslant 100\%$ of the as-measured strength, are generally consistent.

flaws (Fig. 18e, f) and (3) failure from a flaw partly in a second grain (Fig. 18d), i.e. similar to fractographic results of dense, transparent $MgAl_2O_4$.

3.3. Slope and intersections of the $\sigma - G^{-1/2}$ branches

Basic issues to be addressed are the proper G value(s) to use, the slopes of the larger and finer G branches and the intersections with each other and of the large G branch with the σ axis. These are inter-related in that the G value(s) used clearly affect both the slopes and intersections. However, these must be consistent with the mechanics of failure, which are considered in this section as a guide to the appropriate G values. The issues of which G value(s) to use, how to measure them effectively, and ensure that other microstructural and test factors are also consistent and correct, are considered in subsequent sections.

Consider first the slope of the larger G branch. Some investigators using G_m have assumed that (1) the slope of this branch should be the polycrystalline K_{IC} and (2) that this branch passes through the $\sigma - G^{-1/2}$ plot origin. Both assumptions must be wrong. The upper limit of the large G branch is the intersection of it with the finer G branch(es); i.e. when $C \sim G/2$, the polycrystalline K_{IC} may no longer be pertinent. Flaws must often encompass a few grains before the transition from grain boundary or single crystal to polycrystalline K_{IC} values is completed [62]. Hence, for many materials, the transition between the finer and larger G branches may be at less than the polycrystalline K_{IC}. Further, well before $C = G/2$, thermal expansion anisotropy (TEA) stresses can begin to aid failure [63]. This means that for non-cubic materials the apparent K_{IC} (i.e. calculated only from the applied stress at failure) will be $<$ polycrystalline K_{IC}. Similar, but smaller, effects may occur due to

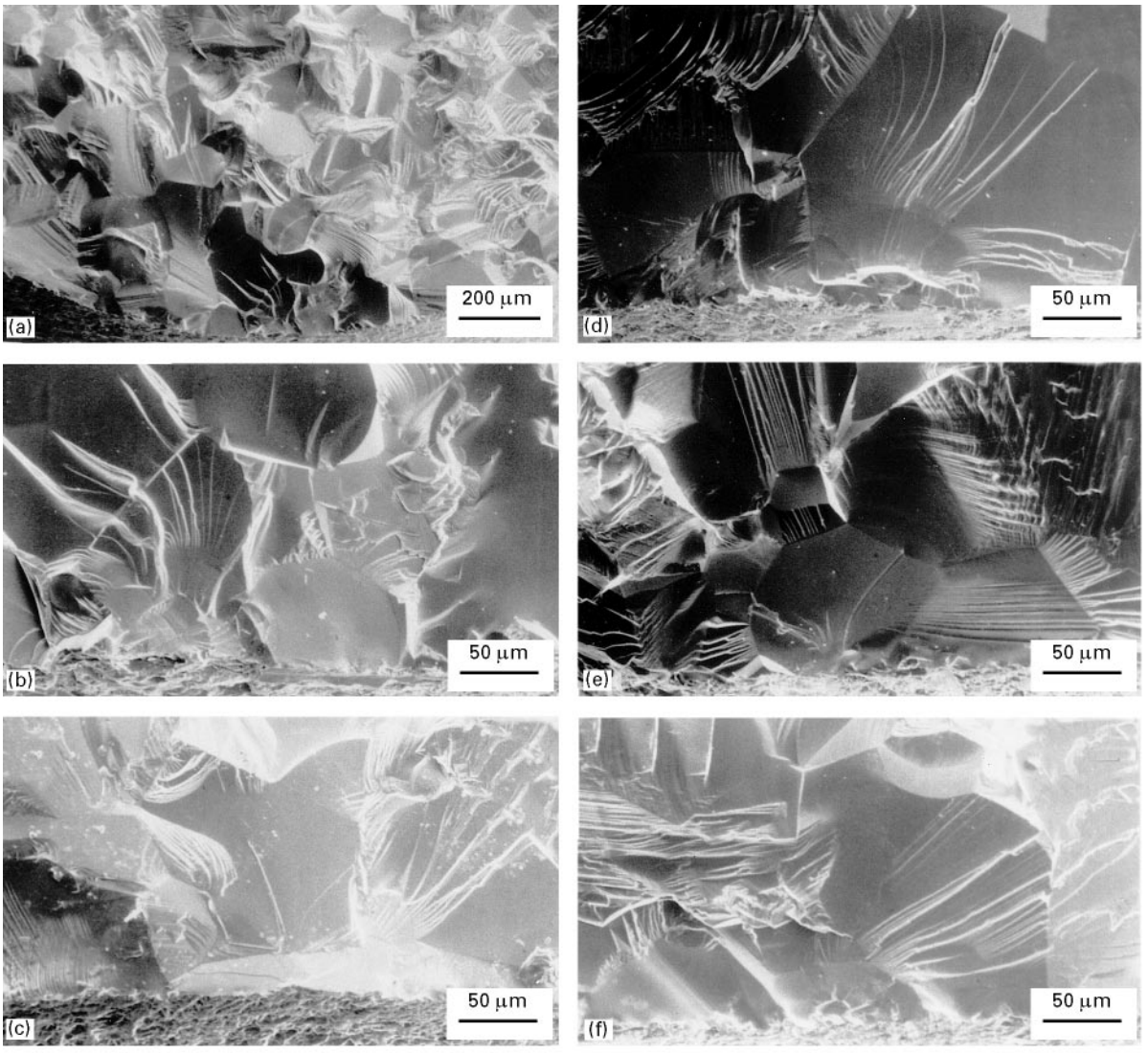

Figure 18 Machining flaw fracture origins in large grain, transparent Y_2O_3 (+10 m/o ThO_2). (a) and (b) lower and higher magnification of the same fracture origin. Note the presence of larger grains near, but not at, the origin in (a), (c)–(f)

elastic anisotropy, EA, which also includes cubic materials.

Proceeding down the larger G branch to larger G and lower σ, two factors further reduce the K_{IC} controlling σ and hence the larger G branch slope. TEA (and EA) effects on failure should continue to increase because flaws are more completely contained within one grain. Even more fundamentally, C continues to decrease relative to G, because it is well established that machining flaws do not differ greatly between single and polycrystalline bodies [5, 64, 65]. Thus, as G continues to increase, the initial C will become progressively less than G. For some range of G, initial (subcritical) flaw growth is limited by individual grains which become the flaw size. Such ultimate control of C and hence σ by G has been theoretically considered [66–68]. Singh *et al.* [66] first considered such subcritical crack growth, showing that this would (1) vary the intersection of the two σ–$G^{-1/2}$ branches from $C \sim G/2$ to $C = 3G$ (in addition to this intrinsic variation of large and finer G branches, intersections can also vary due to varying flaw shape and location relative to the grains, e.g. a flaw may be approximately the size of a grain, but cross the boundary between two adjacent grains, e.g. Fig. 18d) and (2) give large G slope between single crystal and polycrystalline K_{IC} values, depending on whether the transition between these as a function of C/G occurred as a step function or more gradually. Evans [67] subsequently showed that the large G branch could exhibit an intrinsic $G^{-1/2}$ dependence independent of the original C, but with a slope intermediate between the single and polycrystalline K_{IC} values provided the stress–crack length relationship has a maximum and the polycrystalline K_{IC} has no, or limited, G dependence. Virkar *et al.* [68] combined and refined these two analyses noting the need for better definition of the local K_{IC} values, e.g. their dependence on C. These analyses considered only subcritical growth of intragranular flaws (i.e. at single crystal K_{IC}s); intergranular (i.e. grain-boundary) flaws should give still lower K_{IC}s, and slopes. As noted above, observed slopes in this study are all less than the polycrystalline K_{IC} (Table I), as they are in earlier [3] and subsequent [4, 5, 7] studies, where slopes down to approximately single crystal K_{IC} values have been observed consistent with these analyses. The present study (1) is also consistent with the $C \sim G/2$–$3G$ range for the intersection of the

two branches whether the K_{IC} values there are equal to or less than the polycrystalline value there, and (2) shows that investigators claiming the larger G branch slope = K_{IC} [13] are wrong, e.g. incorrectly calculated this using $C = G$ instead of $C = G/2$.

Subcritical crack growth ultimately must no longer reach G, and failure must then be determined entirely by single crystal or grain boundary K_{IC}s. Kirchner and Ragosta [69] estimated that this should begin to occur in Al_2O_3 when $G \sim 200$ μm. Clearly, there must be a transition from polycrystalline to single-crystal strengths, which, except for materials with microplastic control of σ, are higher than many larger G values (Figs 1, 5, 14). This transition (1) may often include a grain boundary (e.g. in some cases a bi-crystal) failure state depending on both material character and test specimen dimensions relative to G, thus giving a variety of transition paths, and (2) means the large G branch slope must decrease, then reverse (Fig. 1). Gentilman's [70] fusion cast, transparent spinel ($2Al_2O_3 . 1MgO$) specimens with large (2–5 mm) G tested with grain boundaries perpendicular to the tensile axis support this transition. K_{IC} measurements affected by multigrain phenomena such as bridging are inappropriate for much, if not all, of this larger G range (and possibly the larger G portion of the finer G regime).

Most investigators plotting σ versus G_m explicitly assumed that finer G branch slopes were 0, i.e. that C and K_{IC} are both independent of G, implying any G would be acceptable. However, there are substantial experimental and theoretical grounds for rejecting this as a general assumption. Extensive experimental data at finer G in this (Figs 2, 3, 6–8, 13) and other studies [1–5, 7] show significant positive finer G slopes. Theoretically, even in the finer G regime, some second-order G effect on machining flaw sizes is expected based upon microstructural effects on crack formation from machining, e.g. models typically give [71]

$$C \propto \left[\left(\frac{P}{K_{IC}}\right)\left(\frac{E}{H}\right)^{1/2}\right]^{2/3} \quad (2)$$

where E is Young's modulus, H the hardness, and P the load on an abrasive particle. Because E normally does not depend upon G, the resultant C will be inversely proportional to differing powers of H and K_{IC}. H typically increases measurably with decreasing G in the finer G region, [4, 72], indicating some reduction in C with decreasing G, hence a positive σ–$G^{-1/2}$ slope. Because K_{IC} is generally approximately independent of G for cubic materials [4] there would be no off-setting effects. However, non-cubic materials commonly have decreasing K_{IC} at finer G [4, 14, 15], so C might decrease less, equal or more, due to K_{IC}–G versus H–G trends, hence giving variable finer G slopes. Such machining effects will normally not be determined by G_m, but G_a values.

A similar C decrease with G can also be expected for as-fired or high temperature annealed surfaces due to grain-boundary grooves. Coble [73] theoretically showed such grooves act a failure-causing flaws of size $G/15$ to $\sim G$. Further, such grooves are less severe for finer than coarser G bodies owing to the relatively lower temperatures, shorter times, or both, used in obtaining finer G. Support for the deleterious effects of grain-boundary grooving or grain faceting – surface roughness at medium G – are indicated by Simpson's [4, 36] Al_2O_3 fibre results, and at fine G by increasing σ of FP fibres $\sim 25\%$ by smoothing their surface with an SiO_2 coating [38–40]. Such grooving while scaling with G, depends on the relative orientations of the two grains forming each boundary, which is not a function of G and hence limits correlation with G_m at large G, i.e. where one or a few boundary grooves determine failure.

More general are the effects of C/G on K_{IC} for fired or machined surfaces. The disappearance of TEA (and possibly EA) effects on σ requires some G range into the finer G branch, as also may transition from completion of the grain boundary, or single crystal, to polycrystalline K_{IC}. This would also yield an initial positive fine G branch(es) slope. Many non-cubic materials show K_{IC} (based on large cracks) decreasing with G over much of the finer G range contrary to σ results, thus showing such K_{IC} do not determine σ.

Other factors may lead to different, or changing finer G branch slopes. Thus, increasing preferred orientation in some BeO with increasing G appears to give a negative finer G slope [74]. More generally at sufficiently fine G, i.e. much less than 1 μm, K_{IC} values may decrease from those of the larger G polycrystalline material (e.g. approaching those for a glass of the same composition due to the disordered grain-boundary structure) which could give negative fine G slopes. Whether the reported decreased K_{IC} at $G < 1$ μm in β-SiC [75] reflects such changes, is not yet known.

3.4. Which G values to use and their impact

In materials with heterogeneous G, the G value to use is determined by G effects on (1) the stress intensity acting on failure-causing flaws, and (2) the fracture toughness of the material ahead of the flaw which will control its critical stage of propagation. G can affect the critical flaw size and character, e.g. shape (especially for non-equiaxed grains as discussed later), and location relative to stress gradients, and hence its stress intensity. G can affect both via basic toughness–G_a dependence and by effects of C/G on (1) contributions of thermal expansion anisotropy (TEA) and related microstructural stresses to failure, and (2) the transition from grain boundary or single crystal to polycrystalline toughness values.

Data pertinent to the finer G branch(es) (Fig. 1) have $C > G$. If there is significant grain heterogeneity such that failure-causing flaws are contained within individual large grains or along their boundaries, such data are pertinent to the large G branch, using G_m, and will generally be of lower σ. However, as shown earlier, this requires not only sufficiently large grains, but also actual association of flaws with them, which is not ensured. (Also, as discussed later, proper use of G_m requires a correspondingly proper σ value.) Otherwise $C > G_m$, especially as G becomes finer (e.g. $\leqslant$ 10–20 μm) and belongs in the finer G branch

because the main effect of G on σ in the finer G branch is via fracture toughness, so use of G_m is clearly inappropriate. Instead an average G will reflect the K_{IC} for the crack to propagate to failure. However, because toughness may be G-dependent, a weighted average of G to reflect G heterogeneity may be appropriate (as discussed later).

Consider next the large G regime where (at least the initial) $C < G$, so as C becomes $\ll G$ (e.g. $G \geqslant$ 100–200 μm) G_m should become less pertinent, as discussed earlier. Thus, the region where G variations are most important is near the intersection of the finer and larger G branches; i.e. at moderate (intermediate) G. While the σ levels do not differ as greatly between the connecting portions of the two branches, as between more extreme portions of the larger and finer G branches, the issue of which G to use is still important, especially if the G data range is limited. However, it must again be emphasized that a clear impact of G_m has only been observed in materials with significant exaggerated, non-cubic grains that provided larger than normal flaws, e.g. as emphasized in Al_2O_3 and B_4C, of this work. Further, though not sought, unequivocal cases have been observed where failure has not occurred from such large grains (Fig. 12). Thus, while failure from larger grains is common in such materials, it is not ensured. Clearly such failure depends on a number of statistical variables such as the association of such large grains and a suitable flaw, and the orientation and location of both relative to high stresses. A clear understanding of the statistics of large grains being the source of failure versus their not being a source, is unknown, because it has not been seriously considered, though previously noted [5]. Further, failure from larger grains does not automatically mean that σ was controlled by their G if the final $C > G$. On the other hand, studies of cubic materials, e.g. MgO [20], Y_2O_3 [62], ZrO_2 [18], and $MgAl_2O_4$ [4, 62] not commonly showing exaggerated grain growth, showed no preference for failure from larger grains within the typical G distribution exposed on fracture surfaces (e.g. a range of approximately threefold). The first of two basic questions with regard to such grain heterogeneities acting as fracture origins is the frequency of its occurrence and hence its effect on σ–$G^{-1/2}$ plots. In the most extreme cases (in Al_2O_3) in this study, up to 40% of the data points of some sets were affected. However, more typically, 10%–20% of the data points were for such failure. Several of these could be rejected because of their low σ values for the average G. Some would also be rejected upon fractographic identification based on their unusual origin character. The main effect of such fractographic examination is thus not a major change in the σ–$G^{-1/2}$ plot, but a shifting of some data points, most commonly at intermediate G and lower σ, to the larger G branch. This thus decreases some of the lower bounds of the finer G branch(es) and shifts the larger G branch to somewhat larger G.

The second basic question regarding origins from large isolated grains or grain clusters is how well they reflect failure in a body of uniform large grains equal to the isolated ones. While failure from large grain clusters may reflect more of the effects of a uniformly large G body within the cluster (but not at the interface with the finer G matrix), if the cluster size, or a significant fraction of it is the origin, then it will often have no relation to σ–G relations. This will usually be manifested by lower σ, e.g. as seen in this study. Further, effects of possible preferred orientation (suggested by spherulitic character, Fig. 4), and the related radial tabular grain structure in some of these clusters must be addressed. Most of the origins involving one or a few large grains in this study were shown to be approximately the expected flaw size (thus reinforcing their being fracture origins) and consistent with other data for G of similar size. Such approximate equivalence should occur where the larger and finer G branches meet which, for normal flaw populations, will be at intermediate G (e.g. 20–50 μm). Thus, origins from isolated larger grains or clusters of them should aid in defining at least the more moderate G region of the larger G branch, where there is less opportunity for substantial deviation. However, there are various factors which can have a bearing on the effects of large grain origins that may be conflicting, but probably most important at larger G. Isolated larger grains acting as origins will not reflect the extreme of TEA stresses that would occur in a body of uniform larger G, with this difference probably decreasing with increasing average G. Similarly, failure from larger grains, where much or all of the failure occurs intergranularly between the larger grain(s) and the surrounding finer G matrix, is likely to be increasingly different from intergranular failure within the finer G matrix itself as the average G decreases. Greater effects of TEA stresses in uniform, large G bodies would imply lower σ and hence somewhat higher, larger G slopes. Such issues are likely to be even more serious where the larger grains are thin platelets (e.g. as seen in some of the hot-pressed Al_2O_3 specimens of this study and that of Tressler *et al.* [8] as indicated by an analysis of Hasselman [76]. His model shows that elastic anisotropy (EA) can lead to stress concentrations approaching the ratio of the maximum to minimum Young's modulus for various crystallographic orientations. Such stress concentrations significantly increase as the extent of grain elongation increases (i.e. as the aspect ratio of tabular grains increases) as well as on the orientation of the elongated grain axis relative to both the grain crystal orientation and the stress axis. Both the aspect ratio and orientation factors introduce inherent statistical variations.

3.5. G measurement and other related characterization

Whatever value of G is appropriate, it must be suitably measured. While measurement of G would appear to be a straightforward application of the standard linear intercept method, closer examination shows this is not the case. This method gives $G = \alpha l$, where l is the average intercept length for grains along a random sample line and α is a constant (commonly ~ 1.5) to account for the fact that neither the sampling lines nor the plane on which they are taken, cut grains at their

true diameters. However, both theory and experiment show α values ranging from < 1 to > 2, due to only partially understood dependencies on grain shape and size distributions [77, 78] and possibly to whether the surface is polished or fractured [79] and the degree of inter-versus trans-granular fracture. Further, there is no precise way to relate such an average G with individual, e.g. G_m, values, because there is no way to relate measurement of a single grain diameter on a sample surface to random grain chords (linear intercepts).

Because fracture is an area-generating, hence area-dependent, process, it may be more realistic, particularly for flaw failure, to relate measurements of σ and K_{IC} to the grain dimensions actually exposed on the fracture surface. Converting a linear intercept measurement to an average surface grain diameter, G_s, might be done using $G_s \sim [(1 + \alpha)/2]\, l$ (i.e. assuming half of the correction, $\alpha - 1$, is due to the randomness of the sampling plane cutting the grains and half of the randomness of the linear intercept itself), but is uncertain in both the form as well as the actual α value. Overall, it appears better to measure actual grain diameters exposed on the fracture surface, e.g. selected by using random lines as in the linear intercept method. Such measurements would be directly related to measuring individual, e.g. largest, grains. Further, having actual diameters of grains allows the calculation of an average G based on various weightings [80]. Because fracture is an area-generating process, weighting based on grain area, i.e. $G = [\sum_n G_i^3][\sum_n G_i^2]^{-1}$ as opposed to diameter, i.e. $G = {}^1/n[\sum_n G_i]$ may be more appropriate. Such an area–weighted average increases the impact of larger grains on average (e.g. in measuring diameters of 30 grains on a commercial, lamp envelope Al_2O_3 the area-weighted and normal G_a were, respectively, 51 and 29 μm).

Unfortunately, many of the specifics of G measurement are not given in the literature. For example, Spriggs and co-workers [81, 82] values are based, not on direct G measurement, but on heat-treatment temperatures and times previously seen to give the indicated Gs (whose determination is not stated). Passemore *et al.* [83] used linear intercept measurements on polished, not fracture, surfaces, but with an unspecified numerical conversion factor, α. Thus, differences between these sets of data and Alford *et al.*'s [13] are, at least in part, due to G measurement methods and not necessarily to the use of G_a versus G_m. Similarly, Tressler *et al.* [8–10] and Virkar and Gordon [12] only state that their G_m values were determined by examining several micrographs; no measurement specifics are given, Alford *et al.* [13] did specify the linear intercept method for their G_a (with $\alpha = 1.65$), but no specifics of their determining G_m are given (except to note that typically $G_m \sim 2$ to 3 G_a). In fact, overall, about 40% of the studies included in this paper gave no specification of how G was measured and a similar per cent indicated linear intercept measurements, but gave no α value (many most likely used $\alpha = 1$). Further, many measurements are made from scanning electron micrographs without correction for distortion due to specimen–beam relations.

Another aspect of G characterization that needs to be addressed is grain shape, especially elongated, e.g. tabular grains. Thus, some using G_m where tabular (α) grains were involved, used the maximum dimension, i.e. length [11]. However, fracture mechanics uses the smaller dimension of an elliptical flaw as C (the larger dimension impacts the flaw geometry parameter). Thus, the length of tabular grains is inappropriate (as is the smallest grain dimension by itself as previously suggested [84]), an intermediate G value is appropriate. A value based on the equivalent circular area of the grain may be a reasonable approximation, i.e. as it is for elliptical flaws of varying excentricity [85]. However, the aspect ratio (and orientation effects) may be important, as indicated by Hasselman's [76] modelling of EA, noted earlier.

Besides grain size and shape, the spatial distribution of grains can also be important, especially if fracture origins cannot, or were not, identified. Systematic spatial variations of G, such as different surface and interior G, e.g. from loss of additives near the surface or machining truncating large surface grains (Figs 4b, f, g, 18c and f) are easier to handle. The more general random or irregular distributions of larger grains (e.g. due to statistical variations in porosity and initial particle size or orientation) indicate the need for statistical methods. Stoyan and Schnabel [86] used a pair correlation approach to address this problem, characterizing the frequency of interpoint distances (e.g. between grain vertices or centres – the latter was preferred). They showed a higher correlation of σ for nearly dense Al_2O_3 bodies with one spatial distribution of the grain size than with G_a ($\sim$ 9–15 μm) itself. Modern stereological tools make such characterization more practical, and potentially applicable to pores and pore–grain associations but again, fractography is the most assured method of addressing this.

Preferred crystallographic orientation of grains can significantly affect σ, e.g. as noted earlier for extruded, sintered BeO (from UOX powders having a significant fraction of needle-shaped BeO grains, and none from nominally equiaxed AOX powders) [87, 88]. Several investigators have shown similar preferred orientation effects from extrusion of Al_2O_3, i.e. increases in σ for fracture perpendicular to the extrusion axis [26, 89, 90]. Similarly, preferred orientation from hot-working Al_2O_3 (press-forging) [3] or MgO (hot-extrusion) [60] can increase σ. Because preferred orientation can occur for several materials and processes [87–94], it raises questions of adequately interpreting data from materials and processes that may have (unexamined) preferred orientation. This is a concern for all extruded materials (i.e. Figs 6 and 14). However, it is of particular concern in the studies of extruded Al_2O_3 and TiO_2 rods of Alford *et al.* [13] (Figs 6 and 14) because of (1) the use of elongated precursor particles (aspect ratio 1.5), (2) small diameter rods, (3) the substantial grain sizes reached via grain growth, and (4) both materials being anisotropic, where orientation effects may be more significant.

3.6. Coordination of σ and G measurements for σ–G studies

A basic requirement of any σ–G model or study is that not only should the G values be appropriate, but also so should the σ values, i.e. the σ and G values used be self-consistent with each other. Typically, σ is based on the outer fibre stress at flexural failure, e.g. as used by all investigators using G_m. Such a maximum σ (σ_m) is basically inconsistent with use of G_m and is often more consistent with use of G_a, because the latter has a moderate to very high probability of being associated with σ_m, while G_m has a moderate to very high probability of being associated with $< \sigma_m$ (thus again indicating lower larger G slopes for those using G_m and σ_m). These probabilities and the errors involved in using G_a or G_m depend on both the size and spatial distribution of G as well as the stressed volume and surface. Smaller volumes under high stresses more likely reflect less deviation from the G_a, i.e. use of three-versus four-point flexure, as well as smaller specimen cross-sections and corresponding shorter spans. Round flexture rods have the smallest stressed volume, but a larger surface area from which surface-related flaws can be activated at variable stress. Data directly comparing round and rectangular rods show round rods to have (often substantially) higher σ [44], indicating that small volume at maximum stress dominates over the variably stressed surface in determining σ. Another basic requirement is that other pertinent specimen factors, e.g. effects of orientation, porosity and impurities, be addressed. Of equal or greater importance is the effect of temperature. A recent review [95] shows that even modest changes in temperature can change σ–$G^{-1/2}$ behaviour in different fashions for different materials, again indicating that a more comprehensive, as opposed to a simplistic, view is needed.

The first and most fundamental of four approaches to properly mesh σ and G values is via fractography. This, if successful, allows both the actual G and the location of fracture initiation to be determined. With the latter the failure stress (if $< \sigma_m$) can be corrected for stress gradients into the sample depth. (Correction for off-centre) failures due to gradients along the sample length, e.g. for three-point flexure, is a separate operation from fractography). However, as noted above, even with fractography there can be considerable uncertainty, hence the need for other approaches. A second approach is statistical, to estimate the probability that G_m or some G significantly more than G_a will be present in a high-stress region possibly to cause failure as discussed earlier. While none of those using G_m have done so, Ting *et al.* [25] and especially McNamee and Morrell [26] did provide some of this information. A third approach is to utilize the stress–volume and surface–area relations noted earlier, i.e. use smaller specimens and stressed volumes more likely to reflect less G variation, so G_a is more reasonable. A fourth approach is to use the known σ–$G^{-1/2}$ behaviour as a guide. This and the other approaches are best when done in combination with one another, e.g. for specimens known to have a range of G, the statistical fit of σ with other data, especially for more homogeneous grain structures, at the pertinent G values, can be used as a guide for the placement of the data points (or their rejection) probably also aided by fractography. Lack of such combinations and comparison has been a serious shortcoming of many earlier studies, including those using G_m.

Application of the above approaches, especially fractography, is illustrated in addressing two issues. First is the question of whether there is a reasonable probability of finding large grain origins that are distinctly internal instead of at the tensile surface in flexure, and hence increasing the probability of larger inconsistencies between σ_m and G_m. This is, of course, fairly frequent in true tension, and has been shown in Al_2O_3 (from large grains with a pore) [21]. However, while dependent on specimen parameters, it is also true in flexure, e.g. in this study in both Al_2O_3 and B_4C (Fig. 11, where the centre of the large grain was ~ 500 μm in from the tensile surface).

Second, consider implications of this work regarding the applicability of crack bridging and resultant R-curve effects on strength–grain-size behaviour, especially of Al_2O_3, because a model of similar strength–grain-size form as shown here, but instead based on bridging-wake effects from thermal expansion anisotropy (TEA), was proposed for Al_2O_3 by Chantikul *et al.* [98]. Because these implications are important, but are not the primary focus of this paper, and are addressed in part elsewhere [15, 95, 99, 100], they are only summarized here. Thus, questions regarding applicability of bridging based on observations of large, arrested cracks, previously propagated at low, unmeasured velocities to cracks controlling strength that are one to three orders of magnitude smaller, accelerate continuously to failure, primarily into the bulk of the material rather than along a free surface, as well as the critical need for fractographic studies have been previously raised [99]. Apparent contradictions between the slopes of the grain-size dependence, especially of the finer grain branch, were noted earlier, and are treated in more detail elsewhere [15, 100]. Great uncertainty in the validity of the proposed TEA-based model due to the similarity of σ–$G^{-1/2}$ behaviour of both non-cubic and cubic materials (the latter without TEA), as shown in earlier studies [3, 5, 7], is further shown in this work, as well as in evaluation of scaling of these σ–$G^{-1/2}$ trends for different materials at 22 °C and the effects of temperature [95]. The σ–$G^{-1/2}$ data of Chantikul *et al.* also raises questions by its agreement with other alumina data, such as in this paper, because their data were obtained by biaxial flexure in contrast to uniaxial flexure for the other data. Thus, because biaxial stresses would appear to reduce frictional effects contributing to bridging effects, why do biaxial and uniaxial stress data agree so well if bridging is a major factor in strength?

Similarly, the greater frequency of bridging due to heterogeneously distributed larger grains has been previously noted [14]. However, the previously raised corollary issue of what spatial distribution of such grains is necessary for them to inhibit failure by making crack extension more difficult, versus fracture

simply avoiding them if they toughen materials, has been previously raised [99]. This is pertinent because brittle fracture is a weak, not strong, link phenomenon, i.e. failure will involve regions of greater toughness only if they are sufficiently numerous that a failure crack cannot avoid them by propagating through regions of less toughness, especially at lower crack velocities during the failure process. However, this (and much other work, e.g. [3, 5, 7]) shows heterogeneously distributed larger grains act as fracture origins rather than being impediments to crack propagation from other origins. More recently, Kovar and Readey [101] have reported lower strengths in unindented versus indented alumina samples with larger and heterogeneously distributed grains, despite the smaller cracks in the unindented samples. They proposed a possible explanation based on *R*-curve effects, but did not consider the simpler possibility that larger, arbitrarily introduced cracks (from indents) may experience more *R*-curve effects, while smaller, natural flaws would experience less or none. (Note that their unindented strengths also agree with the data of this paper.) They originally neglected fractography, but subsequently showed that the unindented fracture origins were larger grains [102] as shown in this and several earlier papers [3, 5, 7]. However, other issues remain, e.g. of reduced opportunities for bridging with fracture initiation from large grains shown here, due to their size and common transgranular fracture (e.g. Figs 4c, d, e, 8–12) or fracture along flat boundary facets, especially of platy grains (e.g. Fig. 4a, b and f) when bridging is highly favoured by irregular intergranular fracture [98]. Similarly, fractures from, or involving, voids (e.g. Fig. 4d and e, and others with much larger pores) raise questions, because pores present no material for wake effects until the fracture propagates into the surrounding solid material [99]. Thus, while bridging is a clearly established and important larger crack phenomena, its applicability to smaller cracks, such as those typically controlling strengths, appears limited, but clearly requires much more specific evaluation, with σ–$G^{-1/2}$ and fractographic evaluations as in this study being important components.

4. Conclusion

The inter-related issues of whether an average or larger, especially maximum, G should be used for σ–$G^{-1/2}$ studies, and resultant finer and larger G branch slopes have been considered at moderate temperatures, mainly 22 °C. This further reinforces the applicability and concepts of the basic σ–$G^{-1/2}$ flaw-failure model; i.e. finer G branches where $C > G$, and a larger G branch where (the initial) $C < G$. The assumption by some investigators that the slope of the larger G branch is equal to the polycrystalline K_{IC}, is not confirmed. Instead, evaluation of experimental data supports theoretical arguments that this slope will be less than the polycrystalline K_{IC}. Arguments are also presented to show that this slope must ultimately reverse sign to complete the transition to single-crystal strengths for flaw (but not slip) initiated failure. Extensive data, as well as theoretical arguments show the slope of finer G branches is generally positive, often substantially so; contrary to the assumptions of some investigators that this slope is intrinsically zero. However, such slopes may vary with processing, including being zero or negative, and may decrease as G decreases, especially at very fine G. While σ–G behaviour can be complex, proper evaluation can limit variations, and is essential for proper understanding of mechanical behaviour and greater material reliability.

With regard to the issue of which G to use, arbitrary use of G_m is inappropriate. Considerable data show separation with regard to material type. Materials not commonly showing exaggerated grain grown (mainly cubic materials such as MgO, Y_2O_3, ZrO_2, and $MgAl_2O_4$) show G_a, not G_m, is appropriate. Materials with exaggerated grains (mainly materials with non-cubic structures or phases, such as Al_2O_3, β-Al_2O_3, Si_3N_4, B_4C and SiC) show some use of larger G values is appropriate, but with complications and limitations. First, the presence of large exaggerated grains is no assurance they will be the source of failure. Though previously not sought, a few clear cases of such large grains not causing failure were shown. How common these are, whether they are material-dependent (e.g. possibly reflecting relief of TEA stresses in B_4C), and the possible role of EA, are not known. Further, failure initiation involving a larger grain is only justified being plotted versus its G value if it dominated failure, i.e. contained the final C, and hence is pertinent to the larger G branch. Larger G origins often violate this. Further, many large G origins are from clusters of larger grains or an association of individual or clustered grains with pores. Many such origins are not fully representative of the basic σ–G behaviour and may need to be rejected (e.g. as also often indicated by their lower σ). Further, even where such larger G failures fit the larger G branch criteria, there are reasons (e.g. due to TEA effects) why they may not fully reflect the same behaviour as bodies of uniform G of the same size. Thus, more testing of large G bodies is needed. Finally, at quite large G (where there are very limited data), G_m may not be pertinent when the size of typical grains is $> C$ (final). Thus a larger, possibly maximum, G value is pertinent to such materials mainly at intermediate and some larger Gs.

The above issue of G values also raises issues of G measurement, other characterization, and their coordination with σ values. The use of G_m is basically inconsistent with use of the outer fibre stress in flexure (e.g. as used by all investigators using G_m) because G_m implies possible failure from regions other than at σ_m. Determining the extent of the possible error in using σ_m with G_m and correction for this can only be done by fractography. Statistical evaluations of the frequency of larger grains (as well as their association with one another and pores) may help, as will the use of smaller test specimens (i.e. to minimize occurrences of such atypical failure), especially where fractography is not practical or effective.

Better measurement and characterization is also important for more accurate analysis of G dependence of σ (and other physical properties). Measurement of the average G diameter on fracture surfaces is

recommended over the common linear intercept method because this allows: (1) statistical weighting of the G value to reflect better the G distribution, and (2) rational comparison of average and other individual G, e.g. G_m, values. For flaw-initiated fracture, it is recommended that the average grain diameter, weight based on grain area, as measured on fracture surfaces (preferably in the origin areas), be used. For tabular or other elongated or irregular grains, the use of the diameter of equiaxed grains of equivalent area on the fracture surface is recommended. However, documentation of grain-shape characteristics (especially length and aspect ratio) for large grain origins may be important for evaluation of possible EA effects. Finally, the issue of grain orientation and its effects, especially in smaller rods extruded from non-equiaxed particles, needs more attention.

Appendix

Strength values are corrected for porosity based on the exponential relationship

$$\sigma = \sigma_0 e^{-bP} \tag{A1}$$

where σ is the strength at volume fraction porosity, P, the subscript zero referring to σ at $P = 0$, and b is a coefficient related to the porosity character. Most b values were those of the original authors or were obtained from their data. Otherwise, b values were estimated as per recent studies [96, 97]. For pores between approximately spherical particles, b ranges from 6 for cubic or approximately random stacking, to 9 for very dense stacking of the particles. For approximately spherical pores, i.e. as is commonly characteristic of intragranular porosity, b is typically 2–3. Because there is typically a mix of the two types of porosity, but intragranular porosity typically increases as G increases, the b value of up to 8 has been used at fine G and moderate P, with b decreasing to 4 as G increases due to increasing intragranular (approximately spherical) pores.

Acknowledgements

The experimental work was performed at The Boeing Co. and the US Naval Research Laboratory.

References

1. S. C. CARNIGLIA, *J. Am. Ceram. Soc.* **48** (1965) 580.
2. *Idem*, *ibid.* **55** (1972) 243.
3. R. W. RICE, *Proc. Br. Ceram. Soc.* **20** (1972) 205.
4. *Idem*, in "Treatise on Materials Science and Technology, Properties and Microstructure", Vol. **11**, edited by R. C. McCrone (Academic Press, New York, 1977) pp. 199–381.
5. *Idem*, *in* "The Science of Ceramic Machining and Surface Finishing II" edited by B. J. Hockey and R. W. Rice, NBS Special Publication 562, (National Bureau of Standards, Washington D.C., 1979).
6. *Idem* in "Fracture Mechanics of Ceramics, edited by R. C. Bradt, D. P. H. Hasselman, and F. F. Lange, Vol. 1 (Plenum Press, New York, 1974), pp. 323–43.
7. *Idem*, to be published.
8. R. E. TRESSLER, R. A. LANGENSIEPEN and R. C. BRADT, *J. Am. Ceram. Soc.* **57** (1974) 226.
9. R. C. BRADT, J. L. DULBERG and R. E. TRESSLER, *Acta Metall.* **24** (1976) 529.
10. D. C. CRANMER, R. E. TRESSLER and R. C. BRADT, *J. Am. Ceram. Soc.* **60** (1977) 230.
11. S. PROCHAZKA and R. J. CHARLES, *Am. Ceram. Soc. Bull.* **52** (1973) 885.
12. A. V. VIRKAR and R. S. GORDON, *J. Am. Ceram. Soc.* **60** (1977) 58.
13. N. McN. ALFORD, K. KENDALL, W. J. CLEGG and J. D. BIRCHALL, *Adv. Ceram. Mater.* **3** (1988) 113.
14. R. W. RICE, "Test-Microstructural Dependence of Fracture Energy Measurements in Ceramics," ASTM Special Technical Publication, **745** (American Society for Testing and Materials, Philadelphia, PA, 1982) pp. 96–117.
15. *Idem*, *J. Mater Sci.* **31** (1996) 1969.
16. *Idem*, "Fabrication and Characterization of Hot Pressed Al_2O_3", US Naval Research Lab., Washington D.C.: NRL Report 7111 (1970).
17. *Idem*, *J. Am. Ceram. Soc.* **73** (1990) 3116.
18. *Idem*, in "Fractography of Ceramic and Metal Failure", edited by J. J. Mecholsky Jr and S. R. Powell, ASTM STP 827 (American Society for Testing and Materials, Philadelphia, PA, 1984) pp. 5–103.
19. *Idem*, in "Advances in Ceramics, **22**, Fractography of Glasses and Ceramics", edited by V. Vrechette and J. Varner (American Ceramic Society, Westerville, Ohio, 1988) pp. 3–56.
20. *Idem*, in "Ceramics for High Performance Applications", edited by J. J. Burke, A. E. Gorum and R. N. Katz (Metals and Ceramic Information Centre, Columbus, OH, 1974) pp. 287–343.
21. *Idem*, *Am. Ceram. Soc. Bull.* **66** (1987) 794.
22. C. D. PEARS and H. S. STARRETT, "An Experimental Study of the Weibull Volume Theory," Technical Report no. AFML-TR-66-228, March 1976.
23. R. W. GRUVER, W. A. SOTTER and H. P. KIRCHNER, "Fractography of Ceramics", Department of the Navy Report, Contract N00019-73-C-0356 (1974).
24. H. P. KIRCHNER, "Strengthening of Ceramics: Treatments, Tests, and Design Applications" (Marcel Dekker, New York, 1979).
25. J.-M. TING, R. Y. LIN and Y.-H. KO, *Ceram. Bull.* **70** (1991) 1167.
26. M. McNAMEE and R. MORRELL, *Sci. Ceram.* **12** (1984) 629.
27. H. P. KIRCHNER, R. M. GRUVER and R. E. WALKER, *J. Am. Ceram. Soc.* **56** (1973) 17.
28. R. W. MISTLER, private communication (1971).
29. R. F. GRUSZKA, R. E. MISTLER and R. B. RUNK, *Am. Ceram. Soc. Bull.* **49** (1970) 575.
30. L. SZTANKOVICS, *Epitoanyag* **42** (1990) 88.
31. C. O. McHUGH, T. J. WHALEN and J. HUMENIK Jr, *J. Am. Ceram. Soc.* **49** (1966) 486.
32. H. TOMASZEWSKI, *Ceram. Int.* **18** (1992) 51.
33. R. J. CHARLES, in "Studies of the Brittle Behavior of Ceramic Materials", Technical Report no. ASD-TR-628 (Aeronautical Systems Division, Wright Patterson AFB, OH, 1962 pp. 370–404.
34. H. D. BLAKELOCK, N. A. HILL, S. A. LEE and C. GOATCHER, *Proc. Br. Ceram. Soc.* **15** (1970) 69.
35. J. E. BAILEY and H. A. BARKER, in "Ceramic Fibres for the Reinforcement of Gas Turbine Blades", Vol. 5, edited by W. W. Kriegal and H. Palmour, III (Plenum Press, New York, 1971) pp. 341.
36. F. H. SIMPSON, "Continuous Oxide Filament Synthesis (Devitrification)", Final report for contract AFML-TR-71-135 (1971).
37. J. D. BIRCHALL, *Trans. J. Br. Ceram. Soc.* **82** (1983) 143.
38. A. K. DHINGRA, in "Contemporary Topics in Polymer Science", Vol. 5, edited by E. J. Vandenberg, Plenum Press, (1984) pp. 227–60.
39. J. C. ROMINE, *Ceram. Eng. Sci. Proc.* **8** (1987) 755.
40. M. H. STACEY, *Trans. J. Br. Ceram.* **87** (1977) 168.
41. D. T. RANKIN, J. J. STIGLICH, D. R. PETRAK and R. RUH, *J. Am. Ceram. Soc.* **54** (1971) 277.
42. P. HING, *Sci. Ceram.* **12** (1984) 87.
43. S. HORI, R. KURITA, M. YOSHIMURA and S. SOMIYA, "Science and Technology of Zirconia III", Advances in Ceramics, Vol. 24A, edited by Shigeyuki Somiya, Noboru Yamamoto, Hiroaki Yanagida (The American Ceramics Society, Westerville, OH, (1988) pp. 423–29.

44. B. R. STEELE, F. RIGBY and M. C. HESKETH, *Proc. Br. Ceram. Soc.* **6** (1966) 83.
45. G. E. GAZZA, J. R. BARFIELD and D. L. PREAS, *Am. Ceram. Soc. Bull.* **48** (1969) 605.
46. A. D. OSIPOV, I. T. OSTAPENKO, V. V. TAROSOV, R. V. TARASOV, V. P. PODTYKAN and N. F. KARTSEV, *Porosh Metall.* **1** (1982) 63.
47. G. DeWITH, *J. Mater. Sci.* **19** (1984) 457.
48. A. V. VIRKAR and R. S. GORDON, *J. Am. Ceram. Soc.* **60** (1977) 58.
49. A. V. VIRKAR, T. D. KETCHAM and R. S. GORDON, *Ceram. Int.* **5** (1979) 66.
50. W. J. McDONOUGH, D. R. FLINN, K. H. STERN and R. W. RICE, *J. Mater Sci.* **13** (1978) 2403.
51. G. J. MAY, S. R. TAN and I. W. JONES, *ibid.* **15** (1980) 2311.
52. R. STEVENS, *ibid.* **9** (1974) 934.
53. J. N. LINGSCHEIT, G. J. TENNENHOUSE and T. J. WHALEN, *Am. Ceram. Soc. Bull.* **58** (1979) 536.
54. T. L. FRANCIS, F. E. PHELPS and G. MacZURA, *ibid.* **50** (1971) 615.
55. H. P. KIRCHNER and R. M. GRUVER, *J. Am. Ceram. Soc.* **53** (1970) 232.
56. J. A. COPPOLA and R. C. BRADT, *ibid.* **55** (1972) 455.
57. S. G. SESHADRI, M. SRINIVASAN and K. Y. CHIA, in "Ceramic Transactions, Silicon Carbide", Vol. 87, edited by J. D. Cawley (American Ceramic Society, Westerville, Ohio, 1989) pp. 215–26.
58. T. D. GULDEN, *J. Am. Ceram., Soc.* **52** (1969) 585.
59. Y. TAKEDA and K. NAKAMURA, in "Proceedings of the 23rd Japan Congress on Materials Science", (Society for Materials Science Japan, (1980) 215–219.
60. D. C. LARSEN, J. W. ADAMS, L. R. JOHNSON, A. P. S. TEOTIA and L. G. HILL, "Ceramic Materials for Advanced Heat Engines: Technical and Economic Evaluation" (*Noyes*, Park Ridge, NJ 1985).
61. R. W. RICE, *J. Am. Ceram. Soc.* **76** (1993) 3009.
62. R. W. RICE, S. W. FREIMAN and J. J. MECHOLSKY Jr, *ibid.* **63** (1980) 129.
63. R. W. RICE, R. C. POHANKA and W. J. McDONOUGH, *ibid.* **63** (1980) 703.
64. R. W. RICE and J. J. MECHOLSKY Jr, in "The Science of Ceramic Machining and Surface Finishing II", edited by B. J. Hockey and R. W. Rice, National Bureau of Standards Special Publication 562 (National Bureau of Standards, Washington D.C. 1979) pp. 351–78.
65. *Idem*, *J. Mater Sci.* **16** (1981) 853.
66. J. P. SINGH, A. V. KERKAR, D. K. SHETTY and R. S. GORDON, *J. Am. Ceram. Soc.* **62** (1979) 179.
67. A. G. EVANS, *ibid.* **63** (1980) 115.
68. A. V. VIRKAR, D. K. SHETTY and A. G. EVANS, *ibid.* **64** (1981) 56.
69. H. P. KIRCHNER and J. M. ROGOSTA, *J. Am. Ceram. Soc.* **63** (1980) 490.
70. R. L. GENTILMAN, *Am. Ceram. Soc. Bull.* **60** (1981) 906.
71. D. B. MARSHALL, in "Fracture in Ceramic Materials-Toughening Mechanisms, Machining Damage, Shock", edited by A. G. Evans, (Noyes, Park Ridge, NJ, 1984) pp. 190–220.
72. R. W. RICE, C. CM, WU and F. BORCHELT, *J. Am. Ceram. Soc.* **77** (1994) 2539.
73. R. L. COBLE, *ibid.* **54** (1971) 59.
74. B. A. CHANDLER, E. C. DUDERSTADT and J. F. WHITE, *J. Nuc. Mater.* **8** (1963) 329.
75. H. KODAMA and T. MIYOSHI, *J. Am. Ceram. Soc.* **73** (1990) 3081.
76. D. P. H. HASSELMAN, in "Anisotropy in Single-Crystal Refractory Compounds", Proceedings of an International Symposium on Anisotropy in Single-Crystal Refractory Compounds", edited by F. W. Vahldiek and S. A. Merool, Vol. 2, (Plenum Press, New York, 1968) pp. 247–65.
77. M. I. MENDELSON, *J. Am. Ceram. Soc.* **52** (1969) 443.
78. N. A. HAROUN, *J. Mater. Sci.* **16** (1981) 2257.
79. E. D. CASE, J. R. SMYTH and V. MONTHEI, *J. Am. Ceram. Soc.* **64** (1981) C-24–25.
80. E. M. CHAMOT and C. W. MASON, "Principles and Use of Microscopes and Accessories, Physical Methods for the Study of Chemical Problems", *Handbook of Chemical Microscopy*, Vol. 1 (John Wiley & Sons, New York, 1938) pp 452–53.
81. R. M. SPRIGGS and T. VASILOS, *J. Am. Ceram. Soc.* **46** (1961) 224.
82. R. M. SPRIGGS, J. B. MITCHELL and T. VASILOS, *ibid.* **47** (1964) 323.
83. E. M. PASSMORE, R. M. SPRIGGS and T. VASILOS, *ibid.* **48** (1965).
84. R. W. RICE, S. W. FREIMAN, R. C. POHANKA, J. J. MECHOLSKY Jr, and C. C. WU, in "Fracture Mechanics of Ceramics", Vol. 4, edited by R. C. Bradt, D. P. H. Hasselman and F. F. Lange (Plenum, New York, 1978) pp. 849–76.
85. G. K. BANSAL, *J. Am. Ceram. Soc.* **59** (1976) 87.
86. D. STOYAN and H.-D. SCHNABEL, *Ceram. Int.* **16** (1990) 11.
87. R. E. FRYXELL and B. A. CHANDLER, *J. Am. Ceram. Soc.* **47** (1964) 283.
88. D. K. SMITH Jr and S. WEISSMANN, *ibid.* **5** (1968) 330.
89. M. J. HANNEY and R. MORELL, *Proc. Br. Ceram. Soc.* **32** (1982) 277.
90. J. A. SALEM and J. L. SHANNON Jr, *J. Am. Ceram. Soc.* **64** (1981) 35.
91. F. V. DiMARCELLO, P. L. KEY and J. C. WILLIAMS, *ibid.* **55** (1972) 509.
92. T. A. WHEAT and T. G. CARRUTHERS, in "Science of Ceramics", edited by G. H. Steward (British Ceramic Society, 1968) pp. 33–51.
93. H. TAGAI, T. ZISNER, T. MORI and E. YASUDA, *J. Am. Ceram. Soc.* **50** (1967) 550.
94. G. ZIEGLER, L. D. BENTSEN and D. P. H. HASSELMAN, *ibid.* **64** (1981) 35.
95. R. W. RICE, *J. Mater Sci.*, submitted.
96. *Idem*, *ibid.* **31** (1996) 102.
97. *Idem*, *ibid.* **31** (1996) 1509.
98. P. CHANTIKUL, S. J. BENNISON and B. R. LAWN, *J. Am. Ceram. Soc.* **73** (1990) 2419.
99. R. W. RICE, *ibid.* **76** (1993) 1898.
100. *Idem*, *J. Mater. Sci.* in press.
101. D. KOVAR and M. J. READEY, *J. Am. Ceram. Soc.* **77** (1994) 1928.
102. *Idem*, *ibid.* **79** (1996) 305.

Received 18 March
and accepted 19 July 1996